Bull Volcanol (2011) 73:789–810
DOI 10.1007/s00445-011-0454-3

RESEARCH ARTICLE

The 512 AD eruption of Vesuvius: complex dynamics of a small scale subplinian event

R. Cioni · A. Bertagnini · D. Andronico · P. D. Cole · F. Mundula

Received: 8 March 2010 / Accepted: 7 January 2011 / Published online: 18 February 2011

Abstract We describe the products of the hitherto poorly known 512 AD eruption at Vesuvius, Italy. The deposit records a complex sequence of eruptive events, and it has been subdivided into eight main units, composed of stratified scoria lapilli or thin subordinate ash-rich layers. All the units formed by deposition from tephra fallout, pyroclastic density currents of limited extent being restricted to the initial stages of the eruption (U2). The main part of the deposit (U3 and U5) is characterized by a striking grain size alternation of fine to coarse lapilli, similar to that often described for mid-intensity, explosive eruptions. The erupted products have a phonotephritic composition, with progressively less evolved composition from the base to the top of the stratigraphic sequence. Based on different dispersal, sedimentological and textural features of the products, we identify five phases related to different eruptive styles: opening phase (U1, U2), subplinian phase (U3 to U5), pulsatory phreatomagmatic phase (U6), violent strombolian phase (U7) and final ash-dominated phase (U8). A DRE volume of 0.025 km^3 has been calculated for the total fallout deposit. Most of the magma was erupted during the subplinian phase; lithic dispersal data indicate peak column heights of between 10 and 15 km, which correspond to a mass discharge rate (MDR) of 5×10^6 kg s^{-1}. The lower intensity, violent strombolian phase coincided with the eruption of the least evolved magma; a peak column height of 6–9 km, corresponding to an MDR of 1×10^6 kg s^{-1}, is estimated from field data. Phreatomagmatic activity played a minor role in the eruption, only contributing to the ash-rich deposits of U1, U4, U6 and U8.

The two most striking features of the 512 AD eruption are the recurrent shifting of the eruption style and the pulsatory nature of the subplinian phase. Basing on a large set of observational data, we propose a model to explain this complex dynamics, also observed in other eruptions of similar scale from Vesuvius and elsewhere. The inbalance between the rates of magma supply and magma eruption may have caused the frequent changes in the eruptive style. Conversely, the high frequency oscillations of magma discharge recorded by the deposits of the subplinian phase were possibly related to cyclic instabilities in the permeability of the low viscosity magma column, which modulated magma fragmentation and discharge.

Keywords Subplinian · Vesuvius · Magma fragmentation · Phreatomagmatism · Eruption dynamics

Editorial responsibility: J. Stix

R. Cioni (✉) · F. Mundula
Dip.to di Scienze della Terra, Università di Cagliari,
Via Trentino 51,
09127 Cagliari, Italy
e-mail: rcioni@unica.it

R. Cioni · A. Bertagnini
Istituto Nazionale di Geofisica e Vulcanologia, sezione di Pisa,
Via della Faggiola 32,
56126 Pisa, Italy

D. Andronico
Istituto Nazionale di Geofisica e Vulcanologia, sezione di Catania,
Piazza Roma 2,
95123 Catania, Italy

P. D. Cole
Montserrat Volcano Observatory,
Flemmings, Montserrat, West Indies

P. D. Cole
Seismic Research Centre,
Trinidad and Tobago, West Indies

Introduction

Mid-intensity explosive basaltic eruptions show a range of eruptive styles, from sustained or pulsating lava fountains

depositing thick blankets of coarse material up to a few kilometers from the vent, to the production and dispersal of large amounts of tephra by sustained plumes over large areas. In contrast to high intensity eruptions, which typically show a quasi-steady phase of sustained discharge throughout the eruption, mid-intensity eruptions are more generally characterized by complex sequences of events and repeated short lived phases of magma discharge (Bursik 1993; Cioni et al. 2000; Morrissey and Mastin 2000; Pioli et al. 2008; Houghton and Gonnerman 2008). While the main processes which control the activity during large eruptions have been extensively studied in terms of physical volcanology and modelling, fewer mid-intensity eruptions have been thoroughly studied in the recent years. In particular, especially in the wake of the prolonged mid-intensity activity shown by volcanoes such as Mt St Helens (1980–1986, and 2004–2008) and Montserrat, West Indies (1995-ongoing), these studies have mainly been concentrated on the eruption of silicic, highly viscous magma and on the transition between dome extrusion and explosive activity. Recently, some authors have focussed on mid-intensity eruptions of basaltic magmas, but mechanisms of magma discharge and fragmentation for these events are still debated (Cashman et al. 2007; Parfitt 2004; Pioli et al. 2008; Houghton and Gonnerman 2008; Wong and Larsen 2010). For this reason, together with direct observations of the eruptive dynamics at ongoing eruptions, the study of deposits for past eruptions represents another important tool for defining the variability of this type of activity.

The history of Somma-Vesuvius over the last 20,000 years has been characterized by a large number of explosive eruptions, showing a large variability in style, intensity, magnitude and eruption scenario. In a recent paper, Cioni et al. (2008) reviewed the style of activity of past eruptions and suggested a distinction into five eruption styles, two corresponding to large scale events (plinian, subplinian I), and the other three which characterize mid-intensity eruptions (subplinian II, violent strombolian and ash emission activity). While much research has so far been spent studying the large Plinian events, less has been done to define the main physico-chemical processes which control the mid-intensity eruptions described at Vesuvius (Arrighi et al. 2001; Andronico and Cioni 2002).

Deposits of mid-intensity eruptions are especially abundant during the last 4,000 years of activity. At least 18 mid-intensity eruptions have been recognized in the period between the two subplinian eruptions of Pollena (472 AD; Rosi and Santacroce 1983; Rolandi et al. 2004; Sulpizio et al. 2005) and 1631 (Rosi et al. 1993; Rolandi et al. 1993). In this paper we describe the products of a subplinian II event which occurred in 512 AD according to historical chronicles, interpreting the complex depositional sequence and the variable features of the juvenile fraction in terms of the different styles of the eruption and of the mechanisms driving magma ascent and fragmentation.

Historical accounts

Historical accounts of Vesuvius activity following the 79 AD eruption are sporadic and discontinuous. Documents dealing with descriptions of ongoing activity after 79 AD have been recently revised by Rolandi et al. (1998) and Principe et al. (2004). However, the main source for a summary of the available information on this period of activity is still represented by the fundamental work by Alfano (1924) and herein we rely mainly on this. In his critical review, Alfano records several contemporaneous accounts which indicate that the first eruption after the large subplinian 472 AD event (the Pollena eruption) took place in the summer of 512 AD. The most famous is a letter of the king Theodericus to the praefectus Faustus dealing with the exemption from taxes for people affected by the eruption.

One of the historical sources that describes the 512 AD event (Paschale Campanum in Stothers and Rampino 1983) mentions that Vesuvius also erupted on November 9 of 505 AD. According to Colucci Pescatori (1986) this report could result from confusion with the 472 AD eruption, which also occurred in November.

Principe et al. (2004) have questioned the date of 512 AD event and proposed instead that the preferred date for the first eruption following the large 472 AD event should be considered the year 536 AD. This suggestion is based on several contemporary accounts describing the darkening of the sky over Constantinople for 12–18 months, accompanied by an unusually harsh winter in Mesopotamia. It seems rather unlikely that a mid-intensity Vesuvian eruption might be the source of a volcanic aerosol of such density and duration. We consider it more likely to be related to a much larger eruption, such as the caldera-forming eruption of Rabaul, Papua New Guinea, dated at about 540±90 AD, as suggested by Stothers and Rampino (1983) and Stothers (1984), or the ultraplinian eruption which may have resulted in the caldera collapse of the proto Krakatau (Wohletz 2000). In addition, Procopius of Caesarea, a Byzanthine historian who was in Naples in 536 AD, refers that in that year, ‘the volcano rumbled, but did not break forth in eruption’ (Alfano 1924; Stothers and Rampino 1983).

As a whole, the historical sources indicate that the most probable time interval for the first eruption after the 472 AD event was during the first 20 years of the sixth century AD. In this paper we prefer to maintain the most common and accepted attribution to 512 AD.

Stratigraphy

Scoria fall deposits ascribed to the 512 AD eruption were first reported by Johnston-Lavis (1884). Rolandi et al. (1998) briefly described the deposits in the type section at Terzigno and drew a cumulative isopach map. In the recent geological map of Vesuvius (Santacroce and Sbrana 2003) the 512 AD deposits were included in the 'San Pietro Pyroclastic Formation' under the acronym of PM1. Cioni et al. (2008) used the acronym 'AS1' (for the Italian "Attivita' Storica", Historic Activity) for the eruption, and classified it as a subplinian II type event.

The stratigraphic sequence of the eruption comprises alternating lapilli and ash beds, which are dispersed generally toward the east. The 512 AD tephra have been recognized and described at about 30 sites, up to a distance of 20 km from the vent (Fig. 1). The deposits directly overlie the ash-rich beds of the final phase of the 472 AD Pollena eruption. No paleosol or strongly humified horizon is present at the top of the underlying Pollena deposits. The contact between the two is characterized by minor reworking and decimetre-sized U-shaped channels and scours. The 512 AD deposits are generally at the base of a complex succession, several meters thick, of ash and lapilli layers which record the activity of numerous eruptions which took place immediately prior to the 1631 AD eruption.

We have subdivided the 512 AD stratigraphic succession into eight units (as defined by Fisher and Schmincke 1984), each generally formed by several beds or laminae, which are discrete in terms of grain size and components. The correlation between the different units is shown in Fig. 1, and all the units are well exposed at the key Section 1 (Figs. 1 and 2), the reference section for the deposits of this eruption. Here we use the terms proximal, medial and distal to refer respectively to those stratigraphic sections on the higher reaches of Mt Somma (approximately 2–4 km from the present crater), on the lower slopes (between 4 and 6 km) or in the surrounding plain (>6 km).

Unit 1

In the most proximal sections (e.g. Sect. 1, 6, Fig. 1) a thin bed up to 1 cm of coarse ash to fine lapilli (U1a) is

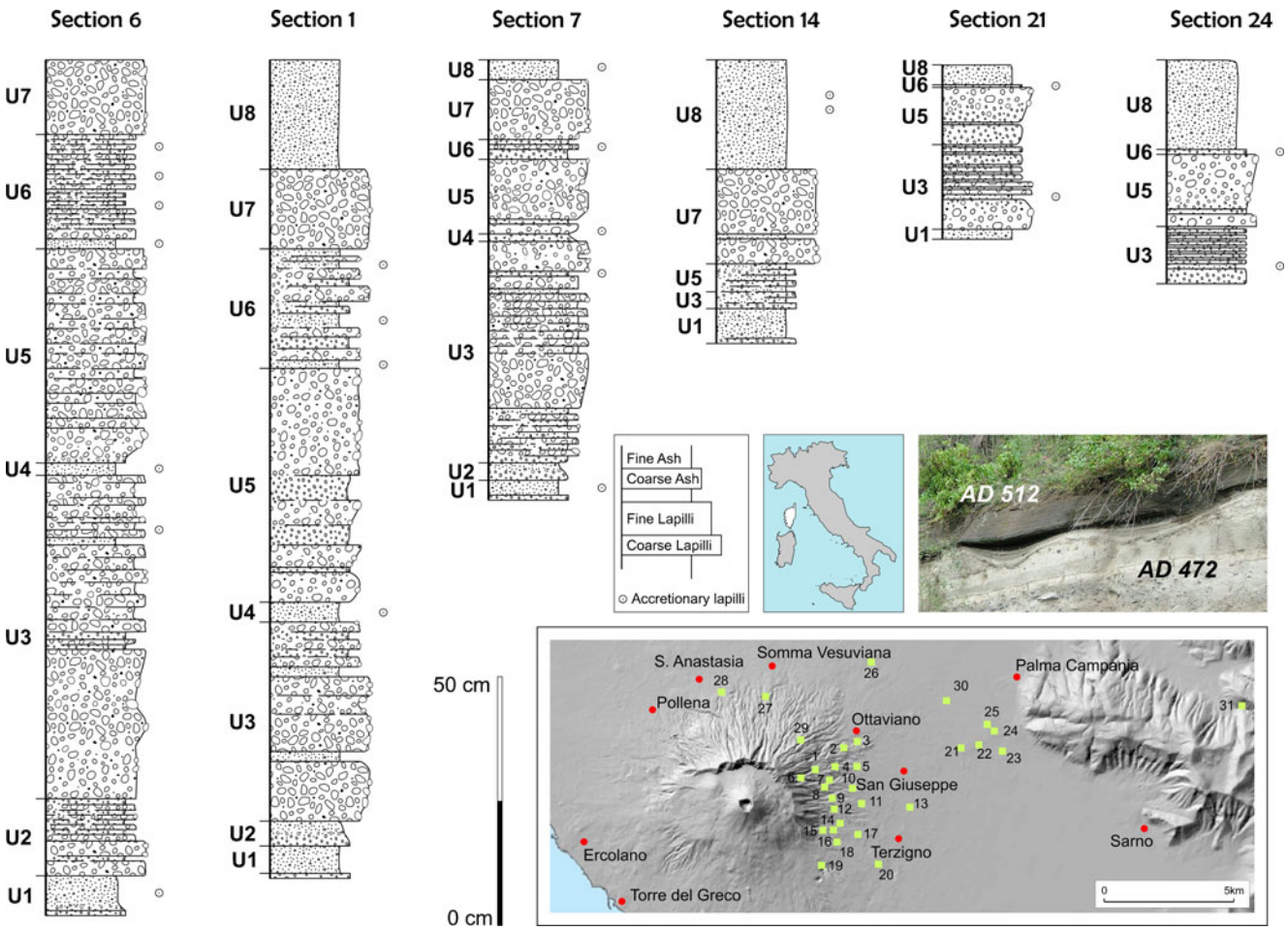

Fig. 1 Selected measured sections through the 512 AD deposit fallout dispersal axis

present at the very base of the sequence. The main part of the unit (U1b) is formed by a faintly laminated, strongly indurated, fine and coarse ash bed with mm-sized accretionary lapilli (Fig. 2a, b). The grain size distribution is polymodal, formed by two or three subpopulations. The coarsest subpopulation (MdΦ = −1.5 to 1, $\sigma\,\Phi$ <1) is related to the accretionary lapilli fraction, while the grain size of the ash is documented by the finer subpopulation (MdΦ=5, $\sigma\,\Phi$=2) (Fig. 3). U1a can be observed up to 4 km east of the present Vesuvius crater, while U1b can be traced up to 6 km east of the volcano with thicknesses variable between 8 cm for the most proximal locations to a few millimetres (Figs. 1 and 4a). Ash from U1 is lithic-rich, with fragments of lava and rare carbonate rocks. Juvenile fragments are generally dense to poorly vesicular, with a microlite-poor, glassy groundmass. Ballistic ejecta formed by lava fragments up to 5 cm in diameter are sparsely present at the base of U1 in the most proximal sites and especially in the southeast sector. The ballistic clasts have locally cut through the reworked fine ash lying on top of the 472 AD Pollena eruption deposits.

Unit 2

This unit is always formed by two subunits (Figs. 1 and 2a, b). The lower subunit (U2a; Fig. 2c) is formed by an alternation of three or four fine-lapilli and coarse-ash laminae. The lapilli are mainly composed of rounded to sub-rounded mm-sized pumice. The upper subunit (U2b) is a normally graded succession of coarse and fine-ash laminae, and is distinguished from U2a by its finer grain size. Both subunits show plane-parallel lamination which grades laterally into 'pinch and swell' structures in the presence of small scale surface roughness. The top of U2b is characterized by small-scale undulations and soft sediment deformation of the fine-ash laminae possibly related to ballistic showers. U2 has a narrow dispersal limited to a 90° wide sector on the eastern slopes of the volcano, becoming indistinct on the surrounding plain at 5–6 km from the present crater (Fig. 4b). The ratio between U2a and U2b thickness rapidly decreases toward the plain and in the northernmost outcrops, where U2 is represented by an accretionary lapilli bearing fine ash which can be correlated with EU2b. U2 componentry is

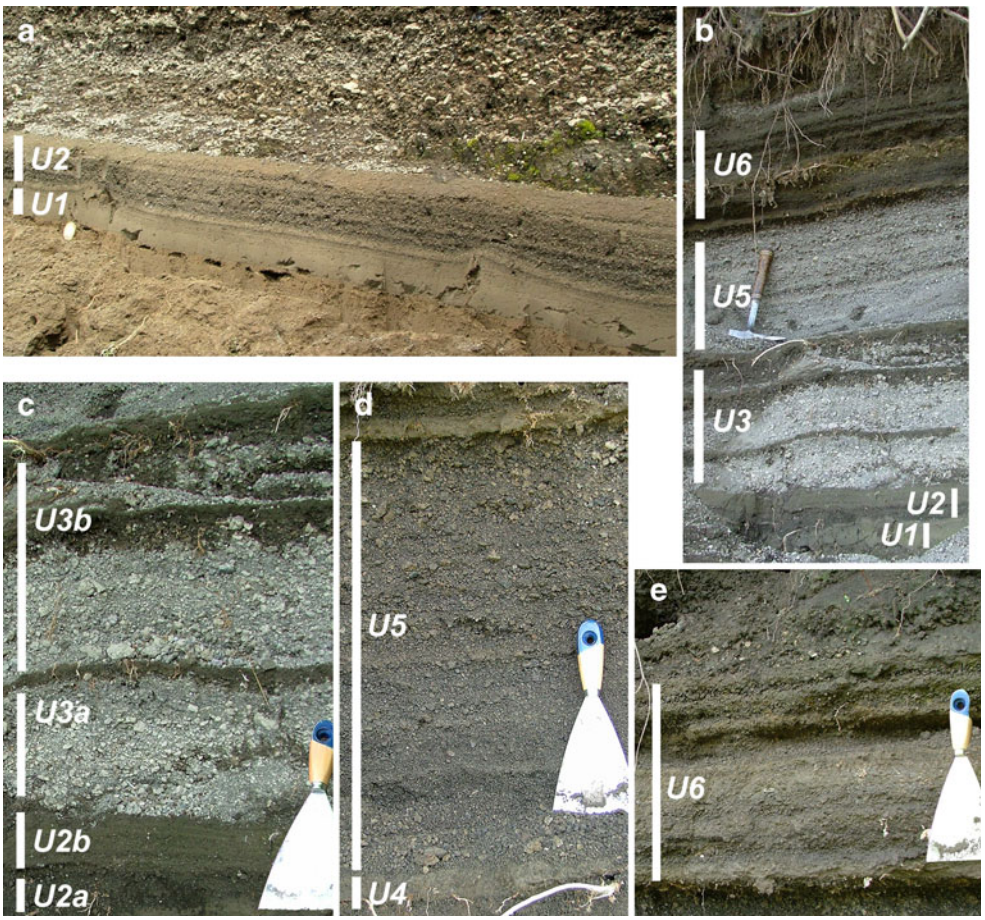

Fig. 2 Photos of the main units at sections 7 (**a**), and 1 (**b**, **c**, **d**, **e**)

dominated by poorly to mildly vesicular, microlite-bearing vitric ash.

Unit 3

Unit 3 is a complex stratified lapilli sequence up to 60 cm thick. In the most proximal sections three lapilli beds are separated by two massive ash beds (Figs. 1 and 2b, c). In the reference section the three coarse grained beds are crudely stratified, owing to well sorted alternations of angular coarse and fine lapilli. In proximal sections accretionary lapilli are locally present in the upper ash bed. The lapilli are mainly represented by irregularly shaped, light brown pumice and angular, dense lithic fragments of pre-existing lavas (about 25% by weight). Ash coating of the pumice lapilli is sometimes present in the lower part of the sequence, suggesting sedimentation of lapilli through an ash-charged cloud. The proximal coarse lapilli sequence grades laterally into a well stratified fine lapilli and coarse ash bed in the medial and distal outcrops. Some of the fine-grained beds of the distal outcrops are formed by vesiculated ash. The ash interbeds have a bimodal grain size (Fig. 3), with a lapilli component, possibly derived from the contamination of the ash by the lapilli beds, and a fine ash component.

The unit is dispersed toward the east-northeast, rapidly thinning from 60 cm at 2 km from the present crater up to 8 cm at 12 km. Isopachs of this unit are asymmetrical, with the northern limit of the unit being more widespread (Fig. 4c).

Unit 4

This unit forms a distinctive marker horizon in the 512 AD sequence (Fig. 2). It is composed of brownish massive, coarse to fine ash with scattered ash-coated lapilli. Subspherical vesicles are present in the ash bed, and mm-sized accretionary lapilli are ubiquitous. The thickness of this unit varies between 4 and 0.5 cm across the exposed area, and it is dispersed over a 100° wide sector in an east-northeast direction (Fig. 4d). U4 has a clear bimodal grain size distribution (Fig. 3), with a coarse mode mainly dominated by accretionary lapilli, and a fine ash mode.

Unit 5

U5 represents the main lapilli deposit of the 512 AD sequence, as it is the thickest and coarsest unit (55 cm and up to -1.4 MdΦ at the reference section, Figs. 1 and 3). It can be subdivided into two main subunits: a lower subunit (U5a) that is finer grained and an upper coarser grained subunit (U5b). Unit 5a displays well-defined, plane parallel stratification formed by alternating coarse and fine lapilli beds (Figs. 1 and 2). In the most proximal sections the lower half of U5a has a distinctive coarse ash layer intercalated within the lapilli beds (Figs. 1 and 2). U5b is a faintly stratified coarse lapilli bed which is represented as a more massive, reversely graded bed in distal sections. In the type section, juvenile material represents 75–80 wt% of the deposit (Fig. 3), composed of angular, light brown pumice and dark grey scoria lapilli. Dark grey scoria increases in abundance upwards through U5b, becoming the sole juvenile material in the topmost 2–3 cm. The shape of the lapilli varies from subequant to tabular, with oversized tabular clasts concentrated in the upper part of U5b. Tabular clasts generally have a smooth, fractured, tortoise-like outer skin, possibly related to syneruptive quenching (Fig. 5).

U5 is dispersed toward the east-northeast with asymmetrical isopachs (Fig. 4e). This may be related to a slight difference in the direction of dispersal of the two subunits.

Unit 6

This unit is composed of alternating thin indurated beds, brown to red in colour, of coarse to fine ash (up to 2–3 cm) and fine, dark grey scoria lapilli. The ash beds, often containing mud vesicles, are massive and contain abundant mm-sized accretionary lapilli and scattered scoria lapilli (Fig. 2d, e). The lapilli beds are normally graded and open-framework; clasts are always coated with mud. The juvenile component is about 80 wt% and is represented by poorly vesicular scoria and minor light brown pumice. U6 is dispersed toward the east-northeast over a narrow zone, showing rapid thinning across the dispersal axis (Fig. 4f). In the most distal sections U6 is represented by a red ash layer only a few centimetres thick.

Unit 7

This unit is a normally graded, open-framework coarse-lapilli bed. The lapilli are formed by about 80 wt% moderately vesicular black scoriae which are generally sub-angular and equant (Fig. 3). Platy fragments similar to those present in U5 occur only at the base of the unit together with the coarsest lithic clasts. In the southernmost sections (Sect 14, Fig. 1) U7 has a lower subunit formed by light coloured pumice covered with fine ash, while the rest of the unit is composed predominantly of dense, dark scoria. Lithics are scarce (<10 wt%), while loose crystals

Fig. 3 Composite stratigraphic section of the 512 AD deposits, showing the grain size of the different units, componentry (X crystals, L lithic fragments, J juvenile fragments), and density data of the lapilli-sized juvenile clasts. In the inset, histogram of the cumulative density data ▶

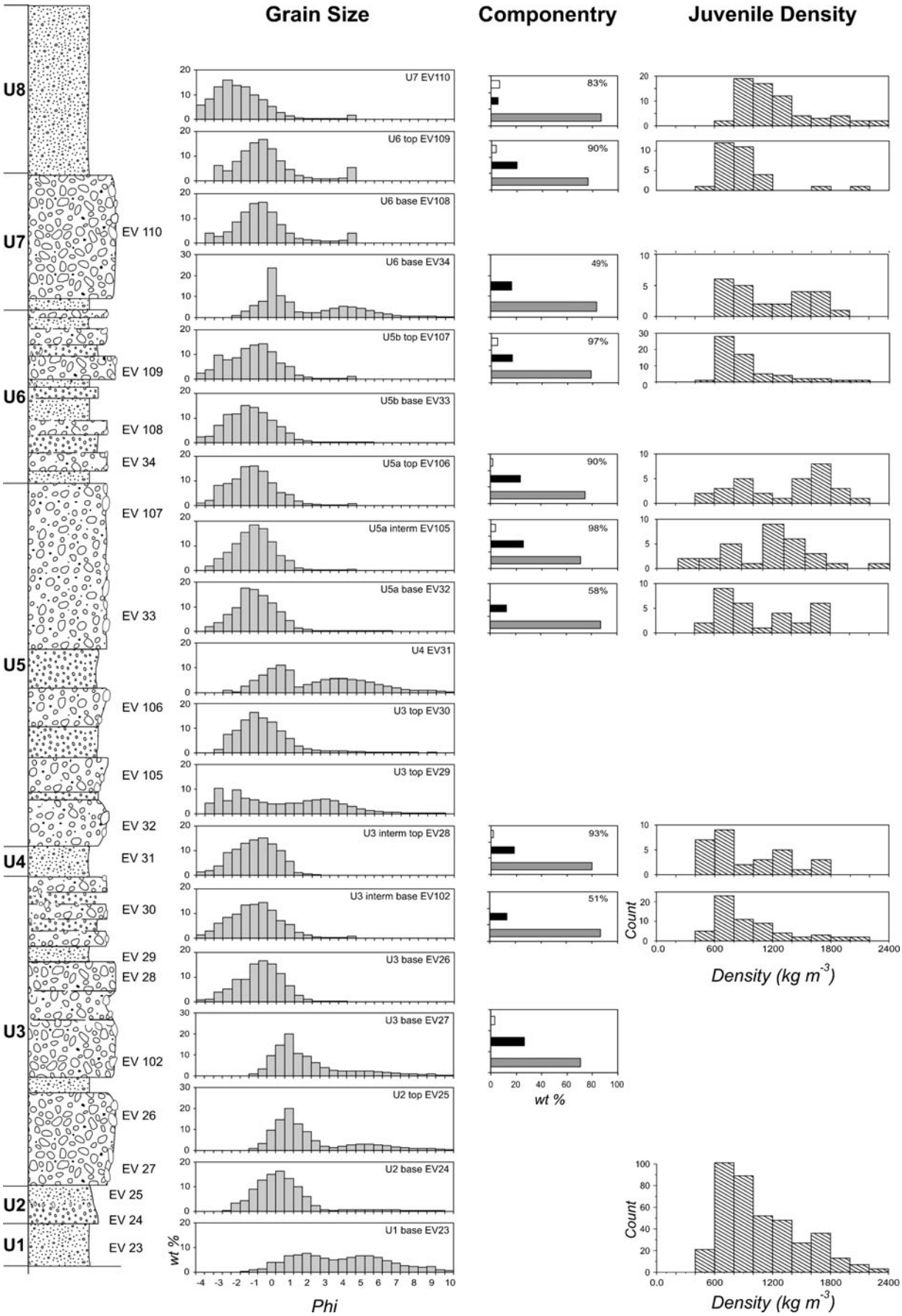
Grain Size
Componentry
Juvenile Density
U8
U7
U6
U5
U4
U3
U2
U1
EV 110
EV 109
EV 108
EV 34
EV 107
EV 33
EV 106
EV 105
EV 32
EV 31
EV 30
EV 29
EV 28
EV 102
EV 26
EV 27
EV 25
EV 24
EV 23
U7 EV110
U6 top EV109
U6 base EV108
U6 base EV34
U5b top EV107
U5b base EV33
U5a top EV106
U5a interm EV105
U5a base EV32
U4 EV31
U3 top EV30
U3 top EV29
U3 interm top EV28
U3 interm base EV102
U3 base EV26
U3 base EV27
U2 top EV25
U2 base EV24
U1 base EV23
wt %
Phi
83%
90%
49%
97%
90%
98%
58%
93%
51%
wt %
Count
Density (kg m-3)
Count
Density (kg m-3)

reach 6 wt%, which is at least twice that present in the underlying units. U7 is widely dispersed over the entire eastern sector (Fig. 4g). It is characterized by an irregular variation of thickness, mainly related to the different dispersal of its two main subunits.

Unit 8

The uppermost unit is mainly present in the southern sections as thick, stratified, alternating coarse and fine ash (Fig. 1) with only rare lapilli. Mm-sized accretionary lapilli form distinct, lapilli-supported layers with local mud vesicles. The stratification is always plane-parallel without any evidence of angular or erosive discontinuities. U8 is dispersed over a wide sector, about 160° wide. The large range of thickness of U8, probably related to post-eruptive erosion, makes it impossible to draw a reliable isopach map.

Grain size and componentry

Grain size analyses were performed on the main beds at the reference section (Sect. 1, Fig. 1). The coarsest beds were analyzed by dry sieving in the laboratories of the Dipartimento di Scienze della Terra of Cagliari (Italy), while the ash beds were analyzed using a laser particle size analyzer at the Geography Department of Coventry University (UK). Grain size parameters were calculated using the SFT software (Wohletz et al. 1989). Most of the analyzed samples show a marked polymodality, generally described by the sum of two gaussian populations: a coarse-grained and a fine-grained population (Fig. 3). The lapilli-bearing units (U3, U5, U7) are formed by >90 wt% of a coarse-grained population with a median between -1 and -2 Φ. All these units have a minor fine-grained population with a peak between 3 and 4 Φ. Conversely, in the ash-bearing units (U1, U2, U4, U6) both a coarse- and

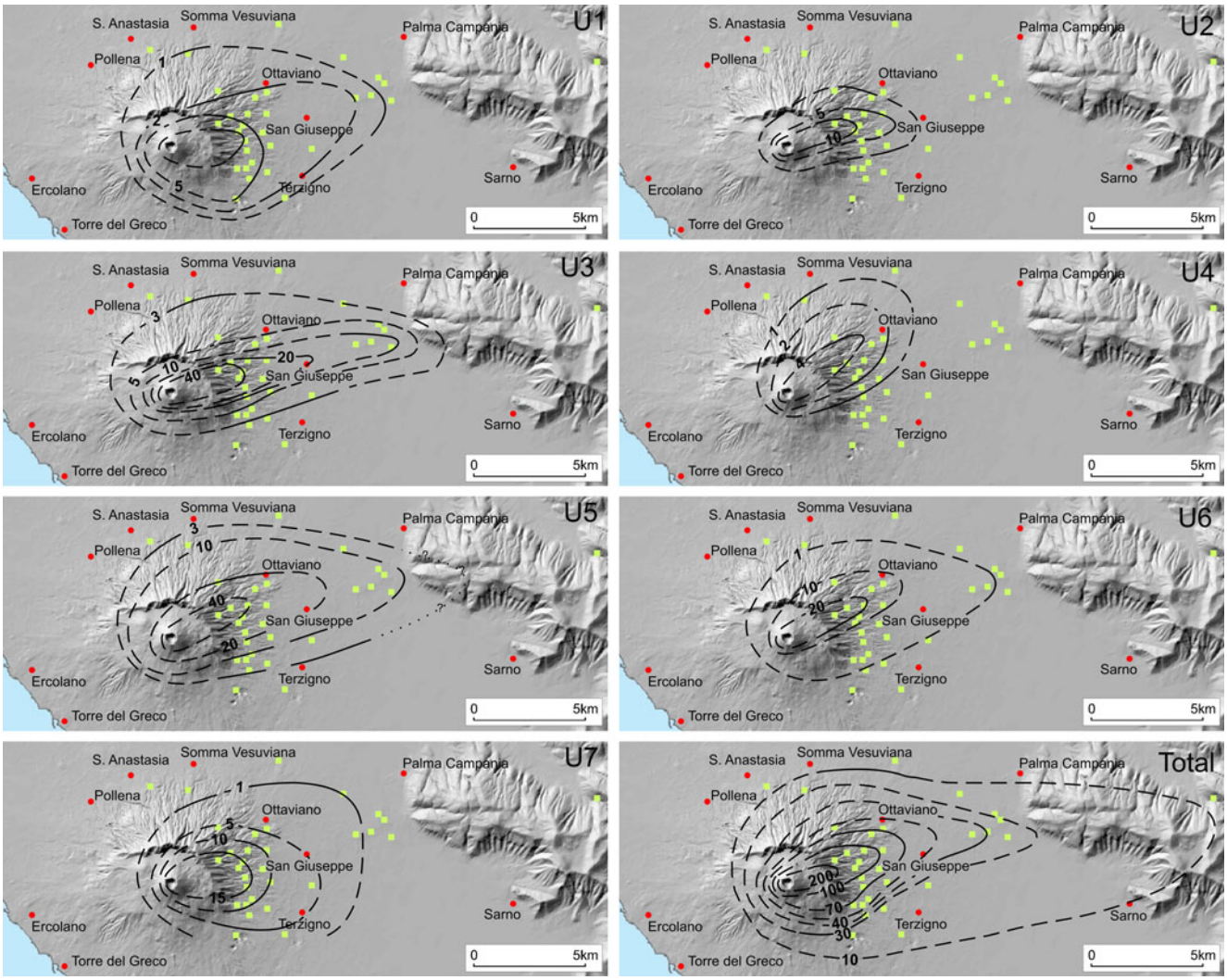

Fig. 4 Isopach maps (in cm) for the different units (U1 to U7) and of the cumulative thickness

a fine-grained population are well represented (Fig. 3). In particular, while the coarse-grained population has a median grainsize similar to that of the lapilli-bearing units, the fine-grained population has a peak between 4 and 6 Φ. In Units 1 and 2, the fine-grained population shows the highest median values, with peaks at 5–6 Φ. Lower values of the median grain size are shown by the fine-grained population of the ash-bearing layers interbedded in Unit 3.

Componentry analysed at the type section shows that juvenile material represents more than 70–80 wt% of the total (Fig. 3), reaching a maximum value close to 90 wt% in Unit 7. Loose crystals are scarce and only present in size classes finer than Φ 1. Lithic material is always less than 25 wt % for the entire sequence, represented by leucite and pyroxene-bearing lava fragments and minor tuffs. Carbonate material is practically absent through the whole sequence, while pieces of intrusive and cumulitic rocks are very rare.

The juvenile fraction

The overall shape and external morphology of juvenile clasts were investigated in order to describe both the variability observed between the different units at the same locality and the variations related to distance within the same unit.

External morphology and surface texture

The juvenile lapilli fraction is characterized by a large shape variability, including equant, prismatic (with flat bounding surfaces) to spheroidal fragments, platy fragments, and strongly convoluted, wrinkled clasts (Fig. 5). Clast vesicularity and vesicle size are both quite variable. The colour of juvenile fragments shows strong variations, ranging from light brown pumice to dark brown to black, vesicular or dense scoria. An important colour change of juvenile material is clearly visible through the stratigraphic sequence, with a progressive increase of the dark material starting from the top of U5, with U7 nearly completely represented by black juvenile material (Fig. 5b). The juvenile lapilli also show a rather large variability in their surface texture. This variability is also observed in the ash fraction and described in the ash morphology section below.

In comparison with other subplinian eruptions of Vesuvius (Rosi et al. 1993; Sulpizio et al. 2005), lapilli with well exposed vesicular surfaces are not abundant among the 512 AD products. Sponge-like textures, characterized by external surfaces of the clasts cutting vesicles, are associated with scoria and rare pumice lapilli, which generally show equant shapes. Highly vesicular, convoluted clasts commonly include dense, juvenile fragments. By contrast, dense fragments never contain low-density inclusions.

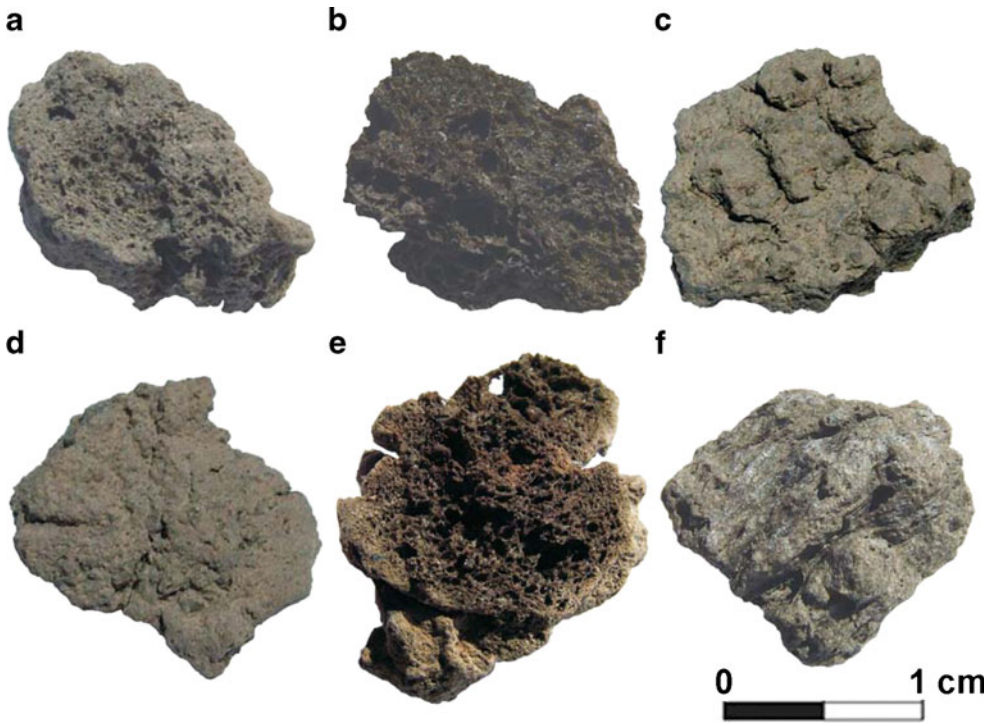

Fig. 5 Different surface and internal textures of the juvenile lapilli; **a** pumice-like, **b** scoria-like, **c** breadcrust texture with orthogonal pattern of fractures, **d** breadcrust texture with radial pattern of fractures, **e** pumice-like fragment with internal gradient of vesicularity, **f** pumice-like fragment with linear stretched vesicles

A typical feature of the 512 AD deposits is the extensive occurrence of lapilli with smooth external surfaces that generally do not intersect vesicles. Two different types of juvenile fragment, with variable relative proportions trough the stratigraphic sequence, are distinguished:

1) Bread crust-like lapilli are characterized by orthogonal or radial fractures. Typically these clasts show platy or platy-convoluted forms (Fig. 5c, d). Convoluted clasts appear to have undergone a thermal wrinkling process. The inner portion of the bread crusted lapilli shows a clear vesicularity gradient from a poorly vesicular rim with small vesicles to a highly vesicular core showing progressively increasing vesicle size (Fig. 5e).

2) Smooth-skinned lapilli are characterized by the presence of smooth, aligned, elongated grooves and ridges parallel to clast elongation (Fig. 5f). They are generally associated with irregular or platy shapes.

Shape factors

The 3D shape of the lapilli fraction was characterized by means of selected shape factors. Around 60 clasts for each sample, randomly picked from the maximum grain size fraction, were measured using a caliper with 1 mm precision. In total, more than 1,700 clasts from the most important units and from different sites were measured using the method of the three orthogonal maximum dimensions (A > B > C).

Several shape factors have been used in the sedimentological literature for clast classification and interpretation (see for example the reviews of Benn and Ballantyne 1993; Illenberger 1991; Hofmann 1994). Of all the proposed diagrams, the shape classification of Sneed and Folk (1958) best represents the variation in measurements. The program Tri-Plot (Graham and Midgley 2000) was used to plot the data and extract the number of clasts plotting in each field of the shape triangle (Fig. 6). For the sake of simplicity, we used only four shape classes (compact, platy, bladed, elongate), simplifying the nomenclature by partially grouping the 10 classes of the Sneed and Folk (1958) classification.

The lapilli units (U3, U5, U7) were sampled at seven different sites. When possible, samples from different stratigraphic levels in the same unit were measured. The most complete sampling was done at the reference section. Important variations of clast shape between the different units are not evident (Fig. 6).

A variation in the abundance of clast shapes with distance is clearly visible from the sections at the foot of the eastern slopes (Sect. 3, Fig. 6) toward the more distal locations (Sect. 24, Fig. 6), with compact shapes forming the most abundant type at more proximal sites to elongate shapes predominating at distal sites.

Bladed clasts are predominant in all the studied samples, rarely representing less than 40% vol. of the total, followed by clasts with elongate shapes comprising generally between 20 and 30%. Platy clasts are abundant (20–30%) only in the proximal section 1 (Fig. 6) and in the off-axis section 18 (Fig. 2). Compact shapes are scarce in the most proximal section, while they tend to be more abundant at medial locations near the foot of the volcano.

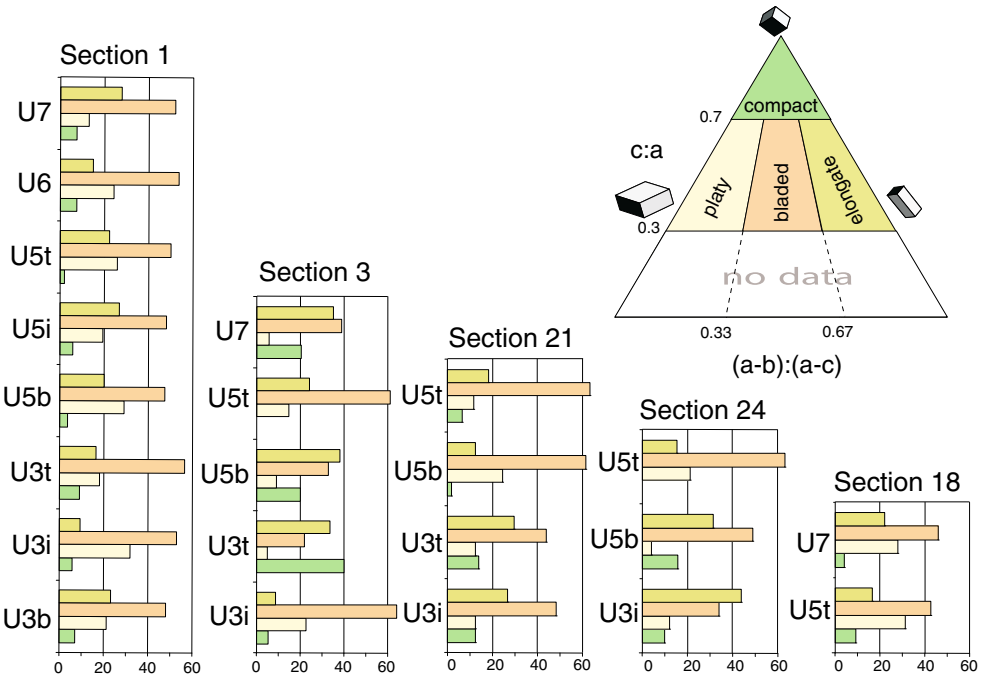

Fig. 6 Bar charts showing the percentage distribution of the different shapes measured for the lapilli-sized juvenile clasts at different sites along the dispersal axis (section 1, 3, 21, 24) and at a site along the margin of the dispersal axis (section 18). The triangular diagram in the upper right is for the legend

Density

The density of about 400 lapilli clasts (Φ from -2 to -4) was measured by hydrostatic weighing on an electronic balance. Clasts were weighed in air, then coated by immersion in paraffin wax, and weighed again in air and water. Clast density was calculated using Archimedes principle. Clast density variation was observed from the base to the top of the type section (Fig. 3). By grouping all the data, a clear bimodality is observed, with a primary, low-density mode peaked at around 750 kg m^{-3} (corresponding to 70% vesicularity) and a secondary, high density mode at around 1,650 kg m^{-3} (34% vesicularity). A third, intermediate mode, peaked at 1,200 kg m^{-3}, is evident from the samples of the lower half of the sequence (Fig. 3). These modes are variably distributed through the deposit sequence; the low-density mode is predominant in all the analyzed samples except in the intermediate level of U5, where the high density mode is most abundant. This high density mode is present in all samples from U5 to the top of the sequence. Conversely, the intermediate density mode is present in Unit 3 and 5, showing a continuously increasing amount with eruption progression. The low-density mode is somewhat shifted toward highest values in samples of Unit 7 (Fig. 3), possibly due to an important change in composition and general shape of the juvenile material.

Ash morphology

Nine samples were selected from the reference section in order to investigate the morphology of the ash fraction during the course of the eruption, as well as between deposits showing a magmatic signature and those with phreatomagmatic characteristics. The 0 Φ fraction was gently rinsed in water in an ultrasound bath for 10 s and dried. A total of 45 clasts from each sample were randomly hand-picked and mounted on a glass slide. The clasts were then studied with a scanning electron microscope in order to characterize their external morphology, vesicularity and possible glass alteration and vesicle filling.

Five main classes of juvenile fragment were recognized: a) spongy, b) blocky dense, c) blocky tubular, d) tubular, e) fluidal (Fig. 7). Spongy clasts have rough, curved surfaces and irregular shapes, mainly determined by the rupture of randomly oriented spherical to ovoid bubbles. The vesicularity is variable from moderate to high. In highly vesicular clasts, bubbles are coalescing with thin walls. Vesicles show less marked coalescence and thicker walls in moderately vesicular fragments.

In blocky clasts the overall shape is prismatic to equant with planar to curviplanar surfaces, chiefly related to the development of large, flattened bubbles originating roughly parallel to surfaces of discontinuity. Blocky dense clasts are incipiently vesicular with ovoid to collapsed vesicles. At higher vesicularities the development of tubular bubbles form the principal characteristics of blocky/tubular clasts.

Tubular clasts have moderate to high vesicularity. They are prismatic in shape with planar to convex surfaces. The most vesicular clasts show highly stretched coalescing bubbles with thin walls ("woody" pumice).

Fluidal clasts are formed by smooth-skinned fragments showing elongate or fluidal forms and curved surfaces that do not intersect vesicles. Vesicularity ranges from incipient to poor, with ovoid to collapsed and/or elongated bubbles. Most of the clasts in this category can be classified as achneliths according to Walker and Croasdale (1972).

Spongy and blocky dense clasts are the most abundant type (40 and 30%) of the analyzed fragments, respectively. They are present in all samples, with percentages varying from 60% to 85% except for U7 (24%). The remaining categories are 13% blocky tubular, 8% tubular and 10% fluidal. Fluidal clasts are practically absent in all analysed samples except for 11% at the base of U5, and for U7 where they reach 72% of the fragments (Fig. 7).

Most of the fragments have adhering dust. The ash coating is extensive for about 30% of the clasts and, in some cases, it completely obscures the original morphology. In the majority of the cases (66%), the ash coating is discontinuous or is mainly present as very fine ash filling vesicles. Dust particles include fresh glass shards and crystal fragments. In some cases, the ash coating appears as crusts, probably due to the presence of secondary minerals. Most of the clasts have entirely fresh glassy surfaces. In about 30% of the fragments, a poorly developed roughness of the surface indicates incipient alteration. Alteration is generally not extensive, but rather concentrated in limited areas.

Bubble textural features

Image analysis shows that bubbles vary greatly through the succession in shape, size and thickness of septa, as well as the presence of collapse and coalescence textures (Fig. 8). U3 clasts (Fig. 8a, b) present bubbles with very irregular outlines and shapes varying from polygonal through ellipsoidal to ovoidal. The thickness of septa is mainly on the order of 1–10 μm. Collapsed bubbles are rare, and bubble coalescence mainly affects the largest bubbles which exhibit cuspidate (wall rupture) re-entrant outlines.

Bubbles in U5 clasts (Fig. 8c to f) show more regular outlines than for the U3 clasts. Thickness of septa is mainly in the order of 10 μm. Collapsed bubbles with a characteristic elongate shape and re-entrant outlines are abundant, and coalescence structures are sometime related with septa retraction.

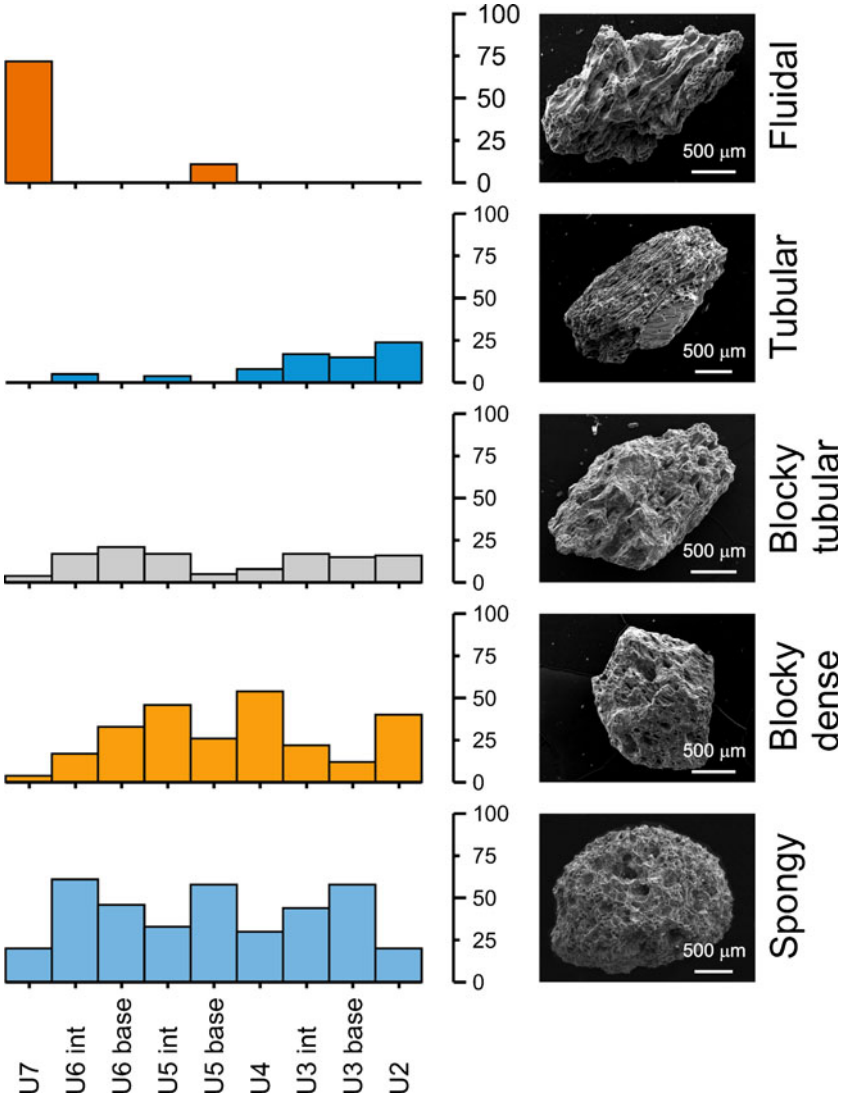

Fig. 7 Variation of the percent abundance of the main types of ash-sized fragments within the stratigraphic sequence

Bubbles in U7 clasts (Fig. 8g to j) present more rounded outlines with respect to the previous samples and abundant sub-circular shapes. Bubble coalescence and structures suggesting bubble collapse are observable in the largest sizes.

Bubble size distribution (BSD)

Vesicle shape and size distribution were investigated in clasts from U3 (two low-density clasts and one high-density clast), U5 (two low-density clasts) and U7 (three low-density clasts) in order to have insights into the modality of magma degassing during the eruption.

Image analysis was performed in the size interval between 1 and 2×10^{-3} mm, using 1 or 2 images at low magnification (25–80x) and 2 or 3 images at high magnification (400–500x) for each clast. The binary images were analysed with Image J software (Rasband 1997), and the area of each bubble section was obtained. Equivalent diameter was calculated from area values in order to plot 2D BSD that was then converted into 3D BSD using the stereological conversion method of Sahagian and Proussevitch (1998) for spherical particles. The abundance of crystals was measured in order to obtain the true 2D vesicularity. Values of the main 3D BSD parameters are shown in Table 1.

The range of bubble size becomes smaller with stratigraphic height as the maximum size decreases and the minimum bubble size increases. In addition, BSD diagrams show the coexistence of two bubble size populations in U3 samples, while both U5 and U7 samples are characterized by a single population. Bubble nucleation density (n_0) generally decreases upsection showing values on the order of 10^7 mm^{-3} in U3, values of 10^7–10^6 mm^{-3} in U5 and values on the order of 10^6–10^5 mm^{-3} in U7. Similarly, bubble number density (N_{tot}) decreases from the base to the

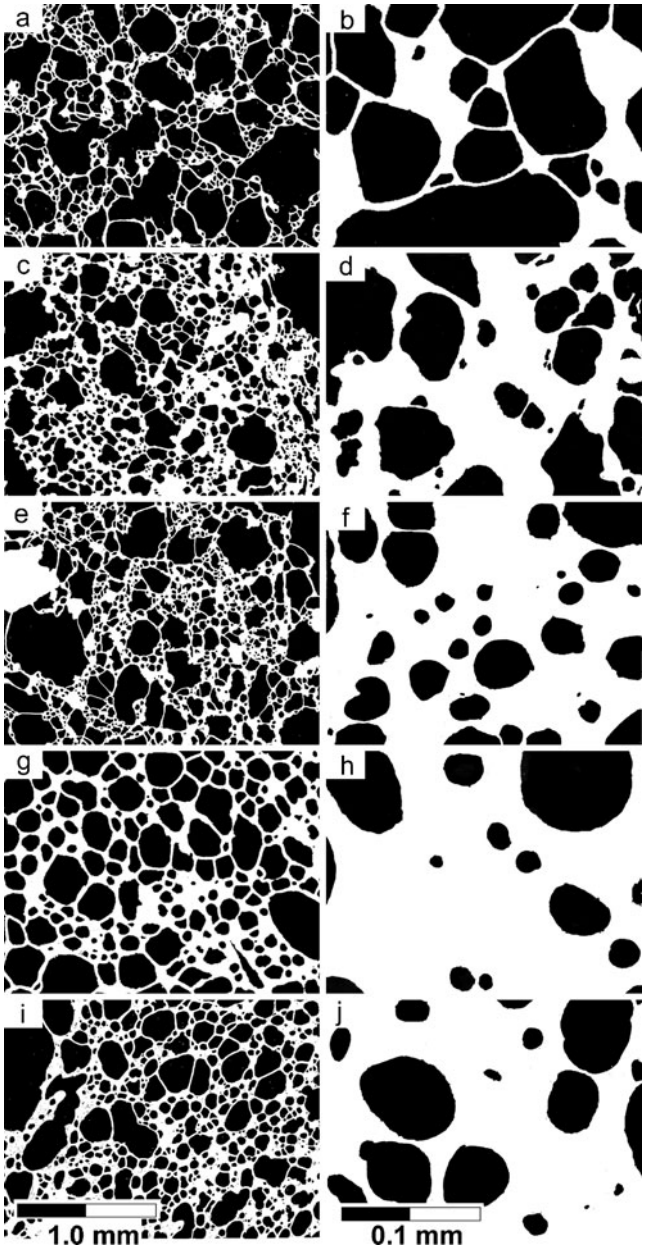

Fig. 8 SEM images in 'binary' format showing the variation of the vesicle shape and size for the stratigraphic sequence (a, b: Unit 3; c to f: Unit 5; g to l: Unit 7)

top of the succession, showing values on the order of 10^6–10^5 mm^{-3} in U3, values on the order of 10^5 mm^{-3} in U5 and values on the order of 10^5–10^4 mm^{-3} in U7. The volume based dominant size Ld ($3G\tau$) increases up the succession from values of 0.091–0.114 mm in U3, to values of 0.137–0.199 mm in U5, reaching 0.201–0.274 mm in U7.

Evidence of wall rupture, irregular and polygonal outlines with cuspidate re-entrant contours, and a scarcity of collapsed bubbles in U3 low-density clasts suggest high decompression rates with bubbles unable to adjust their shape. By contrast, lack of wall rupture, curvilinear outlines, evidence of bubble coalescence and collapse in U5 suggest that magma may have experienced partial degassing before being erupted. The abundance of bubbles with circular shapes in U7 reflects the low viscosity of magma in response to the change in chemical composition. The presence of the two size populations and the large size range shown by bubbles from the clasts of the U3 subplinian phase testify to the pressurized state of the magma reservoir during these first phases of the eruption, during which conditions of bubble nucleation and growth persisted over a prolonged period of time. The presence of collapsed bubbles in U5, together with its single bubble size population, may indicate for a general resorption of pre-existing bubbles during an eruptive hiatus followed by

Table 1 Image analysis data on BSD. See text for symbols

Clast	Vesicularity (crystal free) %	Crystals %	Size range (mm)	n_0	N_v	3Gτ (mm)
U3 high dens.	62	48.4	0.631–0.040	5.26×10^4	5.97×10^3	0.340
U3 low dens.	88	14.2	1.000–0.004	4.32×10^7	1.30×10^6	0.091
U3 low dens.	77	19.0	0.794–0.010	1.07×10^7	4.07×10^5	0.114
U5 low dens	70	9.2	0.316–0.025	1.39×10^7	6.33×10^5	0.137
U5 low dens.	80	27.9	0.631–0.013	2.17×10^6	1.44×10^5	0.199
U7 low dens.	73	38.1	0.631–0.040	1.80×10^6	1.22×10^5	0.203
U7 low dens.	65	28.7	0.501–0.040	1.92×10^5	1.75×10^4	0.274
U7 low dens.	71	39.1	0.398–0.032	1.33×10^6	8.93×10^4	0.201

recompression and a new episode of bubble nucleation. A lower decompression rate is associated with the U7 phase, in which the BSD, characterized by large dominant bubble size and smaller bubble nucleation density, was dominated by high growth rates and low nucleation rates.

Petrography and composition

The phenocryst content of the juvenile material is low (<10 vol %, on a vesicle free basis). Clinopyroxene and rare phlogopite are present as phenocrysts in both dense and highly vesicular fragments, while plagioclase is present only as rare individual crystals in some dense scoria. As is typical in the products of Vesuvian eruptions (Cioni et al. 1998), clinopyroxene shows complex zoning patterns and a wide compositional range, varying from $Wo_{47}Fs_5$ to $Wo_{53}Fs_{30}$. The compositional range of pyroxene phenocrysts is larger in first erupted samples, while in U7 it is restricted into the diopside field. The phlogopite composition is quite variable (Fe/(Fe+Mg) =0.22–0.26). In U7 scoria, phlogopite is only present as rare rounded crystals with dark reaction rims, suggesting a xenocrystic provenance. Leucite is abundant only as microphenocrysts and as microlites. Coarse rounded crystals of leucite are sparcely present, suggesting disequilibrium with respect to the host melt. Apatite and opaque minerals are sporadically present as accessory phases. Phenocrysts are set in a generally vitrophyric groundmass. Groundmass glass varies from hyaline, transparent to opaque, and is oxidized in some dense fragments.

The juvenile products are phonolitic tephrites (SiO_2 48.58–50.42 wt %, Na_2O+K_2O 8.42–10.87 wt %) according to the classification of Le Bas et al. (1986), and show the high alkali content typical of Somma-Vesuvius magmas erupted during the last 2 ka of activity (Cioni et al. 2008) (Fig. 9a, Table 2). Whole rock composition trough the sequence shows a decrease in chemical evolution of the erupted products, indicating that the least evolved products started being erupted at the end of U5 phase (Fig. 10).

Major and trace elements are generally well correlated when plotted against CaO, which was chosen as differentiation index. SiO_2, alkali elements and Al_2O_3, along with incompatible elements, increase with decreasing CaO, while TiO_2, FeO, MgO, and other compatible trace elements (Co, Cr, Ni, V) show a positive correlation. The Th vs. Th/Ta diagram suggests that crystal fractionation was the dominant process controlling evolution of emitted products, and that a direct evolutionary relationship possibly exists between the 512 AD products and those erupted in the previous 472 AD eruption (Fig. 9b). On the basis of the same diagram we can also exclude the intervention of a new mafic magma batch with a contrasting geochemical imprint during the eruption, as for example observed for the 79 AD (Fig. 9b; Cioni et al. 1995). Mass balance calculations (Stormer and Nicholls 1978) give a total fractionated solid (cpx+phl) of around 30 wt%, using the composition of U7 scoria as representative of the least evolved magma and U3 products as the most evolved products. The fractionated solid would consist of 88 wt% clinopyroxene and 12 wt % phlogopite, in agreement with the relative proportions observed for these phases in the products.

Groundmass textural features

Looking at the petrographic features of the clasts, significant textural variability is always present among the different types of lapilli that coexist at the same stratigraphic level. In U3 and U5, vesicular clasts are generally glassy and microlite-poor, in contrast with dense clasts (density around 1,600 kg m^{-3}) that are characterized by a microlite-rich groundmass. Clinopyroxene, leucite and plagioclase, in decreasing abundance, are the only groundmass minerals. The more mafic products of U6 and U7 show a textural variability similar to the underlying units, with a generally greater abundance of

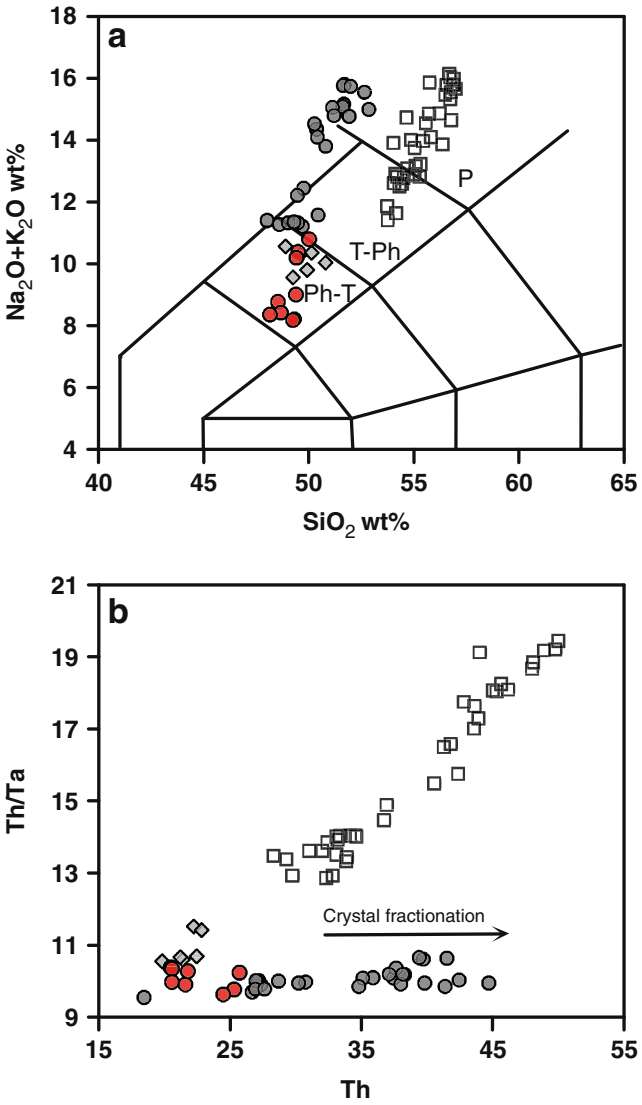

Fig. 9 **a** Composition variability of products emitted in the period 79 AD-512 AD within the Total Alkalis vs. Silica diagram (Le Bas et al. 1986). Squares: 79 AD (Pompeii) plinian eruption; diamonds: explosive activity between Pompeii and Pollena eruptions (Santa Maria cycle); grey circles: 472 AD (Pollena) suplinian eruption; red circles: 512 AD eruption. **b**) Th/ Ta vs. Th diagram (symbols as in Fig. 9a)

clinopyroxene microlites. The compositional range of clinopyroxene microlites is akin to that of phenocrysts, ranging from $Wo_{50}Fs_{16}$ to $Wo_{51}Fs_{22}$ in dense clasts of U3 and from $Wo_{49}Fs_{7}$ to $Wo_{50}Fs_{18}$ in vesicular clasts of the same unit. In U7 the compositions vary from $Wo_{47}Fs_{9}$ to $Wo_{53}Fs_{21}$.

Plagioclase microlites have a rather homogeneous bytownitic composition (An_{76-66}) through the entire succession. The glass composition of the different clast types varies according to microlite content, the most evolved glass being associated with the highest microlite content.

Mingling textures between the two types of clasts are often observed, with microlite-rich, vesicle-poor blebs engulfed in a glassy, vesicle-rich groundmass. The reverse has been never observed.

Physical volcanology

Isopach and isopleth maps were constructed for seven of the eight units which form the 512 AD deposits (Figs. 4 and 11). A total of 28 localities was used, although for some units the number of localities was as low as 15. By integrating the isopachs of the total thickness, total bulk volume for the entire 512 AD deposit is 0.0595 km^3, corresponding to a Dense Rock Equivalent volume (DRE) of 0.025 km^3.

In order to estimate the uncertainty involved in drawing isopach and isopleth maps with a relatively small (but perhaps typical) number of localities, four of us constructed isopach and isopleth maps separately. Volume calculations were then made from the different maps using the single segment method of Fierstein and Nathenson (1992). Volumes from the four different users were then averaged and the variation from these mean volumes for each user calculated (Table 3). For the total isopach volumes, variations between the four authors were up to 22% from the mean. However, for the smaller volumes of individual units, variations increased up to 50% from the mean. Eruption column heights were calculated using the method of Carey and Sparks (1986). The maximum column height (Ht) for the 512 AD eruption is ~10–15 km calculated using the average value of the maximum axis of the five largest lithic clasts from the upper part of unit U5. Results for the lower part of U5 yield heights of 7–12 km (Ht) and U7 6–9 km. As is typical, calculations from the coarse clast sizes (e.g. 3.2 cm) yield lower column heights than those from smaller clasts. Thus, there is considerable uncertainty regarding the true column height from this method. Wind speeds of between 20 and 30 m s^{-1} during the eruption are indicated from the crosswind/downwind range variation.

Previous studies (Pyle 1989; Sparks et al. 1992; Houghton et al. 2000) classified explosive eruptions using values of the 'half distance', the distance over which the deposit thickness or clast size halves (b_t and b_c). Values of b_t for each unit are generally just below 1 (Table 3), but the thickest and coarsest unit is above 1 and the whole deposit has a b_t of 1.41. These values suggest that the 512 AD eruption was of subplinian magnitude. Values of b_c for U5 and U7 are 1.89 and 2.11, respectively, which would also indicate a subplinian magnitude.

Following the relationships detailed in Sparks (1986) the peak mass discharge rates (MDR) of Units 5 and 7 are 5×10^6 kg s^{-1} and 1×10^6 kg s^{-1} respectively.

Table 2 Whole rock (XRF) and glass (SEM-EDS) composition of samples from the different stratigraphic units. In brackets is the number of the averaged analyses for the glass matrix

Sample	AS 94 50	AS 94 51	AS 94 52	AS 94 55	AS 94 56	AS 94 58	AS 94 59	AS 94 60	Matrix glass		
Unit	U3base	U3interm	U3top	U5interm	U5top	U6	U7base	U7top	U3 (4)	U3 (6)	U7 (6)
wt %											
SiO_2	49.08	48.78	48.76	48.86	48.01	48.67	48.13	47.77	48.70	48.37	46.66
TiO_2	0.86	0.91	0.94	0.98	1.03	0.98	1.00	1.02	0.93	0.93	1.24
Al_2O_3	17.94	17.46	17.16	16.41	15.70	14.88	15.65	15.79	20.28	19.32	18.89
Fe_2O_3	3.18	3.42	3.47	3.28	3.59	3.41	3.49	3.79	7.79	7.52	8.54
FeO	4.17	4.27	4.20	4.31	4.41	4.19	4.20	4.25			
MnO	0.16	0.16	0.16	0.15	0.16	0.15	0.15	0.16	0.34	0.15	0.16
MgO	3.09	3.60	3.90	5.04	5.29	6.13	5.94	6.00	1.83	2.91	3.79
CaO	8.09	8.72	8.97	9.83	10.85	11.18	10.82	10.99	7.54	9.15	10.11
Na_2O	3.63	3.46	3.56	2.99	2.85	2.68	2.78	2.73	5.45	4.33	4.30
K_2O	6.95	6.77	6.49	5.91	5.82	5.39	5.55	5.55	6.05	6.36	5.20
P_2O_5	0.51	0.55	0.57	0.68	0.69	0.68	0.72	0.67			
LOI	2.35	1.89	1.83	1.57	1.61	1.67	1.57	1.29			
Total	100.01	99.99	100.01	100.01	100.01	100.01	100	100.01			
ppm											
Zr	267	229	274	229	217	209	211	235			
Sr	1228	1239	1213	1055	1056	989	999	1023			
Rb	289	290	288	268	271	252	255	261			
Ce	144	141.5	141	131.4	130.2	123.5	125.3	129.2			
Ba	1859	1843	1834	1735	1734	1639	1655	1686			
La	72.3	71.1	66.8	63.9	61.2	59.3	58.9	62.7			
Ni	18	23	28	44	53	64	58	59			
Cr	21	36	69	92	138	202	155	162			
Co	21.2	23	24	26.5	28.8	29.1	28.2	29.1			
Sm	10.35	10.31	10.64	10.71	10.52	10.21	10.2	10.7			
Eu	2.59	2.66	2.66	2.75	2.7	2.6	2.56	2.5			
Tb	0.92	0.92	0.95	0.94	0.98	0.94	0.93	0.94			
Yb	2.32	2.43	2.34	2.24	2.49	2.24	2.26	2.19			
Hf	4.98	5.23	5.22	4.92	5.18	4.91	4.96	4.87			
Ta	2.59	2.51	2.54	2.18	2.12	1.97	1.99	2.06			
Th	25.33	25.72	24.48	21.6	21.79	20.46	20.6	20.57			
U	9.44	9.06	9.2	8.3	7.59	7.21	7.47	7.93			

Discussion

The changing behaviour of the eruption

The stratigraphic record of the eruption clearly demonstrates the prevalence of short-lived pulses of magma output compared to long-lived periods of sustained magma discharge. The presence of eight different units, with different dispersal and sedimentological features, also testifies to the occurrence of a repeated variation of eruption style during the event. As with other eruptions at Somma-Vesuvius (see Cioni et al. 2008 for an exhaustive reference list), we have identified five different phases for the 512 AD event, each characterized by distinct eruption styles: opening phase; subplinian phase; pulsatory phreatomagmatic phase; violent strombolian phase; final ash-dominated phase.

The deposition of Units 1 and 2 represents the o*pening phase* of the eruption, which was mainly characterized by ash emission in the form of both convective and collapsing eruptive clouds. The only episode of pyroclastic density current (PDC) generation of the entire eruption corresponds to U2. The rapidly dissipative character of the PDC is well recorded by the relative thickness of the two subunits which form U2, with the coarser-grained, cross-stratified basal subunit thinning rapidly on the slopes of the volcano, while

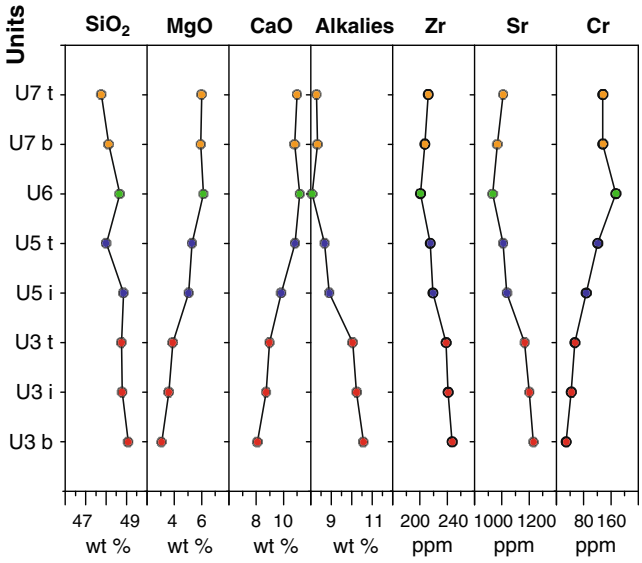

Fig. 10 Vertical variations of some compositional parameters of the juvenile component (Total Alkalis = Na_2O+K_2O)

the finer-grained bed of subunit 2b thickens in the same direction.

The *subplinian phase* corresponds to the deposition of Units 3 and 5, with the prominent formation of oscillating convective columns depositing stratified, normally or reversely graded lapilli fall beds. Magma discharge during this phase was unsteady and probably discontinuous, as the lapilli beds are interlayered with minor ash beds. An episode of phreatomagmatic activity occurred between the two main subplinian phases and is recorded by the accretionary lapilli-bearing U4 deposit.

An important *pulsatory phreatomagmatic phase* is testified by Unit 6. While the phreatomagmatic activity recorded by U4 had possibly high intensity as suggested by its large dispersal up to several kilometres from the vent, the U6 activity was characterized by lower intensity, and the related deposits are only present in the proximal area.

The U7 scoria lapilli bed was emplaced during a *violent strombolian phase*. U6 and U7 scoria corresponds to the emission of the least evolved magma of the entire eruption. The deposits of U7 are limited to the proximal sites, and their strongly asymmetrical distribution could suggest that at least two main lapilli beds were formed during this phase, with a different dispersal (respectively to the east and to the southeast).

The *final, ash-dominated phase* corresponds to the deposition of a thick package (tens of centimetres in the medial outcrops) of laminated fine ash, which possibly records a prolonged phase of ash emission which closed the eruption. Similar phases are present in other eruptions from Vesuvius, of similar (AP1, AP2; Andronico and Cioni 2002) or greater intensity (79 AD, Cioni et al. 1992a; 472 AD, Sulpizio et al. 2005; 1631 AD, Rosi et al. 1993). This type of activity is also well described in several direct accounts of the 1631 AD eruption (Rosi et al. 1993; Bertagnini et al. 2006; Guidoboni 2008).

Factors controlling the variation of the eruption style

The causes of these continuous changes in eruption style are not simple to assess. Many parameters may operate to define the eruption mechanism, such as the magma composition and rheology, the arrival of deep magma in the reservoir, the shape and geometry of the reservoir and plumbing system, and magma/water interaction processes.

Magma composition

Variation of magma composition from the base to the top of the deposit is nearly continuous and defines a trend of progressive alkali decrease and CaO and MgO increase (Fig. 10; Table 2) in the field of phonolitic tephrites. Calculated viscosities of the magma and of the residual melt of the groundmass using the recent model of Giordano et al. (2008) span a restricted range (not more than 2 orders of magnitude) over a large range of eruptive temperature (1,100–1,200°C, Cioni et al. 1999) and water content (0–3 wt%; Fig. 12).

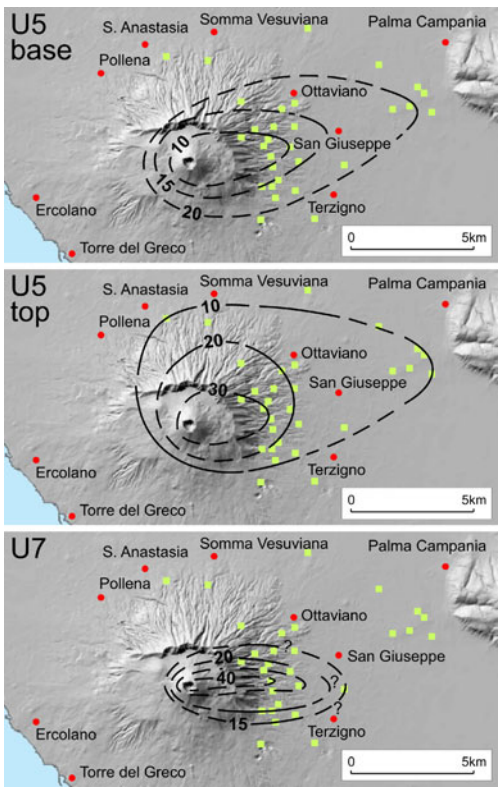

Fig. 11 Isopleth maps (in mm) showing the average of the maximum axis measured for the five largest lithic clasts for the base and the top part of Unit 5 and Unit 7

Table 3 Volume, b_t and b_c data for the different units. For each unit the volume was estimated from isopach maps drawn by four of the authors, to estimate the operator-related uncertainty. The percent difference with respect to the mean value for each unit is also shown

unit	Volume (x10 ^{6} m ^{3})						Bt	Bc
	User 1	User 2	User 3	User 4	Mean	Standard deviation		
U1	3.4	3.6	3.3	2.9	3.3	0.3	0.96	
U1% var from Mean	3.0	10.0	0.0	13.3				
U2	1.7	1.5	2.1	1.4	1.7	0.3	0.61	
U2% var from Mean	0.0	11.8	23.5	17.6				
U3	9.5	8.9	9.1	8.3	8.9	0.5	0.91	
U3% var from Mean	6.7	0.0	2.2	6.7				
U4	1.5	1.2	2.4	1.2	1.6	0.6	0.93	
U4% var from Mean	6.3	25.0	50.0	25.0				
U5	14.5	16.4	19.3	18.5	17.2	2.2	1.08	1.89
U5% var from Mean	15.7	6.1	12.2	7.6				
U6	3.3	3.7	5.1	4.2	4.1	0.7	0.62	
U6% var from Mean	19.5	9.8	24.4	2.4				
U7	5.0	5.0	6.8	4.4	5.3	1.0	0.78	2.1
U7% var from Mean	5.7	5.7	28.3	17.0				
sum of units	38.83	36.70	48.10	40.9	41.13	4.95		
% variation from the mean	5.5	4.4	16.9	0.6				
Isopach of the total deposit	51.7	54.0	72.8	59.4	59.5		1.41	
% variation from the mean	13.1	9.2	22.0	0.16				

The emission of the less evolved, nearly tephritic magma during the final phases (from U6) could be responsible for the generally lower intensity of the violent strombolian phase with respect to the preceding subplinian phase. This could be a result of a change in the fragmentation process related to the decreased viscosity of the erupting magma, possibly also accompanied by a general decrease in the volatile content. This will be addressed in a larger detail in the following.

Possible role of deep magma recharge

The most intense phases of some violent strombolian eruptions at Vesuvius have been ascribed to the arrival of gas-charged, mafic magma from the depth (Santacroce et al. 1993; Marianelli et al. 1999; Marianelli et al. 2005; Scandone et al. 2008). These deep magma batches are recorded by the presence of Mg-rich olivine and diopside with tephritic, volatile-rich melt inclusions. In the case of the 512 AD eruption, however, the general absence of olivine and clinopyroxene with a high Mg-number indirectly suggests that a deep magma input did not trigger the different phases of the eruption. This is also confirmed by the continuous change of the magma composition over the eruption and the previously discussed common line of descent between first and last erupted products.

Geometry of the plumbing system

The variation of the geometry of the shallow plumbing system can exert strong control on magma discharge (Wilson et al. 1980). The syneruptive variation of the plumbing system is typically reflected by changes in the content and nature of the lithic fragments occurring in the deposits (Barberi et al. 1989; Houghton and Schmincke 1989; Varekamp 1993).

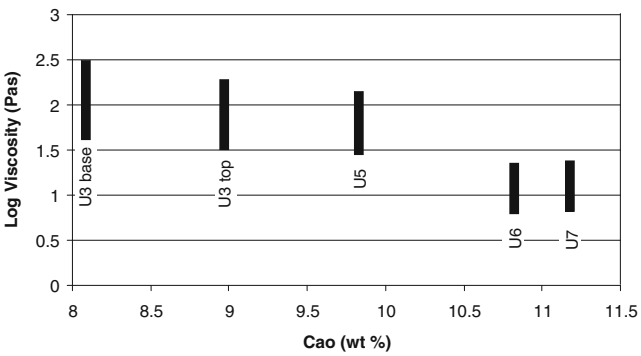

Fig. 12 Calculated variation of magma viscosity along the eruption. Bars show the variability as calculated for a H_2O content variable between 1 and 3 wt. % and temperature of 1200°C (Units 6 and 7) and 1100°C (Units 3 and 5)

Component analysis of the 512 AD products shows a generally low content of lithic material that remains constant throughout the eruption (Fig. 3), indicating that no important changes in the shallow feeding system occurred. The slight decrease in lithic fragments observed in U6 and U7 deposits is consistent with a decrease in the eruptive intensity toward the end of the eruption.

Role of phreatomagmatism

Another potential mechanism that could explain the changes in eruption style is the involvement of surface or phreatic water in the eruption dynamics as suggested by several authors (Schmincke 2004; Morrissey et al. 2000). At Vesuvius, phreatomagmatism has frequently been invoked to explain drastic changes in eruption style occurring during many eruptions (Sheridan et al. 1981; Barberi et al. 1988; Cioni et al. 1992a; Andronico and Cioni 2002; Sulpizio et al. 2005; Cioni et al. 2008). For these cases, the onset of phreatomagmatic activity generally occurred in the final phases; for major events it coincided with phases of caldera collapse (Santacroce et al. 1994; Cioni et al. 1998; Cioni et al. 2008). The occurrence of magma-water interaction has been discounted in other cases, e.g., for the complex subplinian eruption of the Greenish Pumice (Cioni et al. 2003), where the frequent changes in eruption style were interpreted in terms of primary instabilities of magma discharge.

Several studies both at Vesuvius and elsewhere (Heiken and Wolhetz 1985; Barberi et al. 1989; Wohletz 1986; Cioni et al. 1992b; Dellino and La Volpe 1995) have demonstrated that a significant increase in the amount of lithic material, increased fragmentation of juvenile material and lithic fragments derived from aquifer-hosting rocks, and several distinctive morphological features of the juvenile clasts can be considered as good indicators of magma-water interaction, especially when associated with sedimentological features typical of wet deposition (accretionary lapilli; cohesiveness of the bed; soft-sediment deformation).

Data collected on the main Units (U3, U5, U7) of the eruption do not provide a strong argument for an important role of magma-water interaction. In fact, the abundance of highly to mildly vesicular clasts and the dominant ash morphologies (highly vesicular, spongy clasts and mildly to poorly vesicular blocky clasts) are never associated with quenching cracks or strong alteration of the glass, suggesting a primary role of magmatic fragmentation and degassing in the eruption dynamics rather than fragmentation induced (or enhanced) by explosive vaporization of external water. The presence of ash coatings on the clasts trough the sequence is, in our opinion, suggestive of deposition in an ash-charged atmosphere, rather than of ash aggregation favoured by high humidity.

Magma-water interaction possibly occurred during some short-lived phases of the eruption, such as the onset phase U1 as well as U4, which separates the two main subplinian periods of the eruption (U3, U5). A prolonged phase of pulsatory phreatomagmatic activity (U6) occurred at the end of the subplinian phase when periods dominated by deposition of poorly sorted, wet ash repeatedly alternated with periods during which coarse grained, heavily ash-coated scoria lapilli deposited.

Magma supply vs. magma discharge

Moderate-intensity activity is often characterized by a complex dynamics with frequent changes in the eruption style (Orsi et al. 1992; Cole et al. 1995; Hammer et al. 1999; D'Oriano et al. 2005). These eruptions are generally unable to maintain a sustained discharge for periods of several hours, and are recorded by stratified sequences suggestive of the alternating phases of activity and pauses from hours to days. This behaviour suggests a magma supply rate insufficient to maintain a balance with the eruption rate. The low supply rate can be related both to the presence of a narrow conduit system and to low overpressure in the magma reservoir. In the case of the 512 AD eruption, both these conditions were apparently fulfilled. The low lithic content observed in the products is in agreement with a narrow conduit system which was poorly modified during the eruption, while the low overpressure in the magma chamber was possibly an inherited feature of the intense fracturing of the plumbing system left by the preceding caldera forming 472 AD subplinian eruption. The discontinuous magma discharge possibly had a feedback effect on the pressure evolution in the reservoir, promoting significant degassing during the pauses between the different phases, hence preventing a large pressure build up before the next eruptive phase. Magma-water interaction had a minor role in the progress of eruptive activity. Access of external fluids to the magma mainly occurred during the pauses separating the main phases of the eruption, triggering short periods of phreatomagmatic activity with the ejection of a small volume of magma.

Magma composition played an important role only in the final stages, when mafic phono-tephritic magma was made available by the almost complete evacuation of the most evolved part of the magma reservoir. The change in eruption style reflects the important change in rheological properties of the erupting magma, with a decrease of viscosity of at least one order of magnitude.

The pulsatory behaviour of the subplinian phase

While intrinsic properties of the deep magma system possibly controlled the large scale variations in the

eruption, shallower processes were probably responsible for the pulsatory behaviour of the subplinian phase recorded by thinly spaced grain size variations in the two main fallout units (U3, U5). The absence of PDC deposits interlayered in the fallout beds rules out the possibility that these alternations result from a transitional regime of the eruption, characterized by the coexistence of partially collapsing convective plumes and sustained plumes (Di Muro et al. 2004). We thus interpret the repeated grain size variations as related to primary oscillations in the magma discharge. This behaviour has been frequently observed and discussed in low flow rate eruptions of highly viscous silicic magmas. Oscillations in the discharge during this type of activity have been related to several causes, such as stick-slip effects along the conduit (Denlinger and Hoblitt 1999), forced deformation of the conduit by the rising magma driven by syn-eruptive, degassing-induced crystallization (Wylie et al. 1999; Costa et al. 2007) or important rheological changes in the slowly ascending magma, mainly related to decompression-driven degassing (Sparks 1997). The deposits of violent strombolian and small-scale subplinian activity, at Vesuvius and elsewhere, commonly show this typical oscillatory behaviour, despite they are associated with less viscous magmas (Arrighi et al. 2001; Pioli et al. 2008; Cioni et al. 2008, Cioni et al. 2003). In the case of the 512 AD eruption, the calculated low viscosity and the low microlite content of the magma imply that the discharge instability is not caused by syneruptive changes in the viscosity, and could be related to intrinsic instabilities during the process of magma fragmentation.

Data on macroscopic and microscopic features of juvenile clasts allow to put some constraints on the processes of magma fragmentation. External morphology of the lapilli-sized clasts is dominated by smooth-skinned, fluidal surfaces, bladed to platy shapes, and frequent evidence of post-fragmentation expansion (breadcrusted surface, internal gradient of vesicularity). Conversely, ash-sized juvenile fragments are dominated by spongy clasts, showing a generally unimodal vesicle size distribution. The scarcity of lapilli with external surface cross-cutting vesicles suggests that fragmentation was essentially driven by expansion and tearing apart of the liquid magma along the internal surfaces of the larger vesicles. Textural observations and the abundance of platy to bladed-shaped lapilli also suggest that large vesicles were generally elongate. These features are consistent with a low-viscosity magma experiencing rapid ascent under a marked lateral velocity gradient, being able to shear the melt and deform vesicles before reaching glass transition. The ubiquitous presence of dense, blocky-shaped, microlite-rich clasts throughout all the main phases of the eruption suggests that the process of magma rise and fragmentation remained constant throughout the eruption. They possibly represent material from an external collar of magma rising along the conduit, which experienced a slower rise with strong shearing (as in the case of a Hagen-Poisseuille flow), allowing time for degassing and crystallization. This portion of magma was passively disrupted by fragmentation of the inner part of the magma column. This also explains the presence of dense juvenile material within the pumice-like clasts but not vice versa.

Brittle fragmentation of magma by strain rate dependent effects (Dingwell 1996; Papale 1999) or internal vesicle overpressure (Sparks 1978; Alidibirov and Dingwell 2000) results in vesicular fragments with broken vesicles which are exposed on the external surfaces of the clasts (pumice or spongy clasts). The scarcity of this texture in coarsest clasts suggests that the fragmentation mechanism was possibly driven by the inertia of the gas flux acting on a deformable, highly fluid melt. The elongate shapes of the fragments and of the larger vesicles are strongly suggestive of permeability development in the magma during its ascent (Klug and Cashman 1996; Blower et al. 2001). The vesicularity threshold needed to reach an effective permeability is not well established for low-viscosity melts. However, the large proportion of high-vesicularity clasts (~70 vol%) in all the samples suggests that high permeability was probably reached during this eruption. We suggest here that the observed instabilities in magma discharge could reflect the cyclical crossing of a permeability threshold during eruption. Repeated changes in permeability during the subplinian phase may have resulted in unsteady gas loss from the foamy melt, allowing conduit pressure to oscillate and rapidly changing the exit conditions of the mixture.

Conclusions

We have studied the deposits of the 512 AD eruption, based on a detailed description of stratigraphy and sedimentological features (grain size and componentry), including the morphology, textural features, density and composition of the juvenile fraction. This has allowed us to reconstruct the eruption dynamics and the main physical parameters which controlled the temporal evolution of the eruption.

1. The 512 AD deposits are subdivided into eight units, all of which involve fallout. Many of the units are characterized by stratification formed by alternating layers of variable grain size from scoria lapilli to subordinate thin, ash-rich layers. Only one unit (U2) shows evidence of deposition from a pyroclastic density current of limited dispersal. We identify five phases: opening phase, subplinian phase, pulsatory phreatomagmatic phase, violent strombolian phase and final ash-dominated phase. This is evidence of the

complex alternation of different styles of activity which characterize this type of eruptions at Vesuvius and possibly elsewhere (Bursik 1993; Cioni et al. 2000).

2. Based on a reconstruction of the isopach maps of the different phases of the eruption, we estimate that the 512 AD event erupted a total of 0.025 km^3 of magma, although there is considerable uncertainty (at least 30%) based on different users drawing isopach maps. Magma discharge rates of $1–5\times10^6$ kg s^{-1} and corresponding column heights of 10–15 km are estimated for the subplinian phases of the eruption (U3 and U5). The magnitude and intensity for this eruption are one order of magnitude lower than other subplinian events at Vesuvius (e.g., the 472 AD and 1631 eruptions). On the basis of this observation, Cioni et al. (2008) proposed that this and other similar eruptions of Vesuvius form a different category of subplinian events, called Subplinian II events.
3. The juvenile material ranges between 70 and 90 wt% in the analysed beds, while the lithic content is low (generally <10 wt%) and does not vary dramatically through the course of the eruption. The density of the juvenile fraction is bimodal with a low-density peak at 750 kg m^{-3} and a high density peak at 1,650 kg m^{-3}. The coarse juvenile fragments show a variety of morphologies and shapes; typical features are bread-crusted lapilli with platy or convoluted forms, and platy to irregular, smooth-skinned lapilli, all containing elongate, irregularly shaped, large vesicles. Conversely, the morphology of the ash fraction is mainly represented by microvesicular, spongy and blocky/dense clasts (60–80% by volume), with tubular and fluidal ash being mainly present in the uppermost units. These data suggest that the internal structure of the magma column before fragmentation was dominated by large, elongate vesicles forming high permeability channels and separated by variably vesicular, magma portions.
4. The shape distribution of the juvenile clasts does not vary systematically trough the sequence, but varies with distance from the vent. As a consequence, platy clasts are more abundant near the vent, whereas equant to elongate clasts dominate at more distal sites, suggesting that caution must be used when selecting samples to describe the intrinsic variability of the juvenile material.
5. The most striking features recorded by the 512 AD stratigraphic sequence are the recurrent shifting of the eruption style (well recorded by the different sedimentological features of the eight Units) and the pulsatory nature of the subplinian phase (recorded by the grain size alternation of the U3 and U5 deposits). We propose that the frequent changes in the eruptive style through the course of the eruption, were mainly controlled by a magma supply rate not sufficiently high to balance the eruption rate (possibly due to the presence of a narrow conduit system and to low overpressure in the magma reservoir). The pulsating behaviour of the subplinian phase was instead possibly related to frequent instabilities in the shallower part of the magma system and in the nature of magma fragmentation and discharge, which could reflect repeated variations of the permeability (and hence pressure) of the magma column. Phreatomagmatic activity only played a very minor role. We suggest that a combination of these processes described for the 512 AD eruption could be responsible for the complex behaviour commonly shown by similar mid-intensity eruptions.

Acknowledgements The research was done with the contribution of the EC EVR1-CT-2002-40026 Exploris project (Responsible Augusto Neri) and from funds from the Istituto Nazionale di Geofisica e Vulcanologia and Dipartimento Protezione Civile (Project V3-4 Vesuvius) to Raffaello Cioni. Dr Lucia Corsini is greatly acknowledged for field and analytical work, and Patrizia Pantani for graphic assistance. FM acknowledges the Fondazione Banco di Sardegna for founding his research fellowship. We greatly acknowledge the precious suggestions of John Stix, Marc Antoine Longpré and an anonymous reviewer.

References

Alfano GB (1924) Le eruzioni del Vesuvio tra il 79 ed il 1631 (studio bibliografico). Napoli, Scuola Tipografica Pontificia per i figli dei carcerati

Alidibirov M, Dingwell DB (2000) Three fragmentation mechanisms for highly viscous magma under rapid decompression. J Volcanol Geotherm Res 100:413–421

Andronico D, Cioni R (2002) Contrasting styles of Mount Vesuvius activity in the period between the Avellino and Pompeii Plinian eruptions, and some implications for assessment of future hazards. Bull Volcanol 64:372–391. doi:10.1007/s00445-002-0215-4

Arrighi S, Principe C, Rosi M (2001) Violent Strombolian and sub-Plinian eruptions at Vesuvius during post-1631 activity. Bull Volcanol 63:126–150. doi:10.1007/s004450100130

Barberi F, Navarro JM, Rosi M, Santacroce R, Sbrana A (1988) Explosive interaction of magma with ground water: insights from xenoliths and geothermal drillings. Rend SIMP 43:901–926

Barberi F, Cioni R, Rosi M, Santacroce R, Sbrana A, Vecci R (1989) Magmatic and phreatomagmatic phases in explosive eruptions of Vesuvius as deduced by grain-size and compositional analysis of pyroclastic deposits. J Volcanol Geotherm Res 38:287–307

Benn DI, Ballantyne CK (1993) The description and representation of particle shape. Earth Surf Proc Land 18:665–672

Bertagnini A, Cioni R, Guidoboni E, Rosi M, Neri A, Boschi E (2006) Eruption early warning at Vesuvius: The A.D. 1631 lesson. Geophys Res Lett 33:L18317. doi:10.1029/2006GL027297

Blower JD, Mader HM, Wilson SDR (2001) Coupling of viscous and diffusive controls on bubble growth during explosive volcanic eruptions. Earth Planet Sci Lett 193:47–56

Bursik M (1993) Subplinian eruption mechanisms inferred from volatile and clast dispersal data. J Volcanol Geotherm Res 57:57–70

Carey S, Sparks RSJ (1986) Quantitative models of the fallout and dispersal of tephra from volcanic eruption columns. Bull Volcanol 48:109–125

Cashman KV, Mckay D, Pioli L, Rosi M, Rust A, Wallace P (2007) A new classification system for basaltic eruptions. IUGG General Assembly, Perugia

Cioni R, Marianelli P, Sbrana A (1992a) Dynamics of the AD 79 eruption: Stratigraphic, sedimentological and geochemical data on the successions of the Somma-Vesuvius southern and eastern sectors. Acta Vulcanol 2:109–123

Cioni R, Sbrana A, Vecci R (1992b) Morphologic features of juvenile pyroclasts from magmatic and phreatomagmatic deposits of Vesuvius. J Volcanol Geotherm Res 51:61–78

Cioni R, Civetta L, Marianelli P, Métrich N, Santacroce R, Sbrana A (1995) Compositional layering and syneruptive mixing of a periodically refilled shallow magma chamber: the AD 79 Plinian eruption of Vesuvius. J Petrol 36:739–776

Cioni R, Marianelli P, Santacroce R (1998) Thermal and compositional evolution of the shallow magma chambers of Vesuvius: Evidence from pyroxene phenocrysts and melt inclusions. J Geophys Res 103:18,277–18,294

Cioni R, Marianelli P, Santacroce R (1999) Temperature of Vesuvius magmas. Geology 27:443–446

Cioni R, Marianelli P, Santacroce R, Sbrana A (2000) Plinian and subplinian eruptions. In: Sigurdsson H, Houghton B, McNutt SR, Rymer H, Stix J (eds) Encyclopedia of volcanoes. Academic, San Diego, pp 477–494

Cioni R, Sulpizio R, Garruccio N (2003) Variability of the eruption dynamics during a subplinian event: the Greenish Pumice eruption of Somma–Vesuvius (Italy). J Volcanol Geotherm Res 124:89–114. doi:10.1016/S0377-0273(03)00070-2

Cioni R, Bertagnini A, Santacroce R, Andronico D (2008) Explosive activity and eruption scenarios at Somma-Vesuvius (Italy): towards a new classification scheme. J Volcanol Geotherm Res 178:331–346. doi:10.1016/j.jvolgeores.2008.04.024

Cole PD, Queiroz G, Wallenstein N, Gaspar JL, Duncan AM, Guest JE (1995) An historic subplinian/phreatomagmatic eruption: the 1630 AD eruption of Furnas volcano San Miguel, Azores. J Volcanol Geotherm Res 69:117–135

Colucci Pescatori G (1986) Osservazioni su Abellinum tardo antica. App.: Fonti antiche relative ad eruzioni vesuviane ed altri fenomeni vulcanici successivi al 79 D.C.. Treblement de terre, eruptions volcaniques et vie des hommes dans la Campanie antique. Biblioteque de l'Institut Français de Naples Iis, vol VII, Napoli, 134–141

Costa A, Melnik O, Sparks RSJ, Voight B (2007) Control of magma flow in dykes on cyclic lava dome extrusion. Geophys Res Lett 34:L02303. doi:10.1029/2006GL027466

Dellino P, La Volpe L (1995) Fragmentation versus transportation mechanisms in the pyroclastic sequence of Monte Pilato—Rocche Rosse (Lipari, Italy). J Volcanol Geotherm Res 64:211–231

Denlinger RP, Hoblitt RP (1999) Cyclic eruptive behavior of silicic volcanoes. Geology 27:459–462

Di Muro A, Neri A, Rosi M (2004) Contemporaneous convective and collapsing eruptive dynamics: the transitional regime of explosive eruptions. Geophys Res Lett 31:L10607. doi:10.1029/2004GL019709

Dingwell DB (1996) Volcanic dilemma: flow or blow? Science 273:1054–1055

D'Oriano C, Poggianti E, Bertagnini A, Cioni R, Landi P, Polacci M, Rosi M (2005) Changes in eruptive styles during the A.D. 1538 Monte Nuovo eruption (Phleagrean Fields, Italy): the role of syneruptive crystallization. Bull Volcanol 67:601–621. doi:10.1007/s00445-004-0397-z

Fierstein J, Nathenson M (1992) Another look at the calculation of fallout tephra volumes. Bull Volcanol 54:156–167

Fisher RV, Schmincke H-U (1984) Pyroclastic rocks. Springer, Berlin Heidelberg New York

Giordano D, Potuzak M, Romano C, Dingwell DB, Nowak M (2008) Viscosity and glass transition temperature of hydrous melts in the system CaAl2Si2O8–CaMgSi2O6. Chem Geol 256:203–215. doi:10.1016/j.chemgeo.2008.06.027DOI:dx.doi.org

Graham DJ, Midgley ND (2000) Graphical representation of particle shape using triangular diagrams: an Excel spreadsheet method. Earth Surf Proc Land 25:1473–1477

Guidoboni E (2008) Vesuvius: A historical approach to the 1631 eruption "cold data" from the analysis of three contemporary treatises. J Volcanol Geotherm Res 178:347–358. doi:10.1016/j.jvolgeores.2008.09.020DOI:dx.doi.org

Hammer JE, Cashman KV, Hoblitt R, Newman S (1999) Degassing and microlite crystallization during the pre-climatic events of the 1991 eruption of the MT. Pinatubo, Philippines. Bull Volcanol 60:355–380. doi:10.1007/s004450050238

Heiken G, Wolhetz K (1985) Volcanic Ash. University of California Press, Berkeley

Hofmann HJ (1994) Grain-shape indices and isometric graphs. J Sed Res A64(4):916–920

Houghton BF, Schmincke H-U (1989) Rothenberg scoria cone, East Eifel: a complex Strombolian and phreatomagmatic volcano. Bull Volcanol 52:28–48

Houghton BF, Gonnerman HM (2008) Basaltic explosive volcanism: constraints from deposits and models. Chemie der Erde Geochemistry 68:117–140

Houghton BF, Wilson CJN, Pyle DM (2000) Pyroclastic fall deposits. In: Sigurdsson H, Houghton B, McNutt SR, Rymer H, Stix J (eds) Encyclopedia of volcanoes. Academic, San Diego, pp 555–570

Illenberger WK (1991) Pebble shape (and size!). J Sed Petrol 61:756–767

Johnston-Lavis HJ (1884) The Geology of Monte Somma and Vesuvius, being a study in Vulcanology. Q J Geol Soc London 40:35–149

Klug C, Cashman KV (1996) Permeability development in vesiculating magmas: implication for fragmentation. Bull Volcanol 58:87–100

Le Bas MJ, Le Maitre RW, Streckeisen A, Zanettin R (1986) A chemical classification of volcanic rocks based on the total alkali-silica diagram. J Petrol 27(3):745–750

Marianelli P, Métrich N, Sbrana A (1999) Shallow and deep reservoirs involved in magma supply of the 1944 eruption of Vesuvius. Bull Volcanol 61:48–63. doi:10.1007/s004450050262

Marianelli P, Sbrana A, Métrich N, Cecchetti A (2005) The deep feeding system of Vesuvius involved in recent violent Strombolian eruptions. Geophys Res Let 32:L02306. doi:10.1029/2004GL021667

Morrissey MM, Mastin LG (2000) Vulcanian eruptions. In: Sigurdsson H, Houghton B, McNutt SR, Rymer H, Stix J (eds) Encyclopedia of volcanoes. Academic, San Diego, pp 463–475

Morrissey MM, Zimanowski B, Wohletz K, Buettner R (2000) Phreatomagmatic Fragmentation. In: Sigurdsson H, Houghton B, McNutt SR, Rymer H, Stix J (eds) Encyclopedia of volcanoes. Academic, San Diego, pp 431–445

Orsi G, D'Antonio M, De Vita S, Gallo G (1992) The Neapolitan Yellow Tuff, a large-magnitude trachytic phreatoplinian eruption: eruptive dynamics, magma withdrawal and caldera collapse. J Volcanol Geotherm Res 53:275–287

Papale P (1999) Strain-induced magma fragmentation in esplosive eruptions. Nature 397:425–428

Parfitt EA (2004) A discussion of the mechanisms of explosive basaltic eruptions. J Volcanol Geotherm Res 134:77–107. doi:10.1016/j.jvolgeores.2004.01.002

Pioli L, Erlund E, Johnson E, Cashman K, Wallace P, Rosi M, Delgado Granados H (2008) Explosive dynamics of violent Strombolian eruptions: the eruption of Parícutin Volcano 1943–1952 (Mexico). Earth Plan Sci Lett 271:359–368. doi:10.1016/j.epsl.2008.04.026

Principe C, Tanguy JC, Arrighi S, Paiotti A, Le Goff M, Zoppi U (2004) Chronology of Vesuvius activity from A.D. 79 to 1631 based on archeomagnetism of lavas and historical sources. Bull Volcanol 66:703–724. doi:10.1007/s00445-004-0348-8

Pyle DM (1989) The thickness, volume and grain size of tephra fall deposits. Bull Volcanol 51:1–15

Rasband WS (1997) ImageJ. U. S. National Institutes of Health, Bethesda,Maryland, USA, http://rsb.info.nih.gov/ij/

Rolandi G, Barrella AM, Borrelli A (1993) The 1631 eruption of Vesuvius. J Volcanol Geotherm Res 58:183–201

Rolandi G, Petrosino P, McGeehin J (1998) The interplinian activity at Somma-Vesuvius in the last 3, 500 years. J Volcanol Geotherm Res 82:19–52

Rolandi G, Munno R, Postiglione I (2004) The A.D. 472 eruption of the Somma volcano. J Volcanol Geotherm Res 129:291–319. doi:10.1016/S0377-0273(03)00279-8

Rosi M, Santacroce R (1983) The A.D. 472 "Pollena" eruption: volcanological and petrological data for this poorly-known, Plinian-type event at Vesuvius. J Volcanol Geotherm Res 17:249–271

Rosi M, Principe C, Vecci R (1993) The 1631 Vesuvius eruption. A reconstruction based on historical and stratigraphical data. J Volcanol Geotherm Res 58:183–201

Sahagian DL, Proussevitch AA (1998) 3D particle distributions from 2D obsevations: stereology for natural applications. J Volcanol Geotherm Res 84:173–196

Santacroce R, Sbrana A (2003) Geological map of Vesuvius 1:15, 000 scale. SELCA, Firenze

Santacroce R, Bertagnini A, Civetta L, Landi P, Sbrana A (1993) Eruptive dynamics and petrogenetic processes in a very shallow magma reservoir: the 1906 eruption of Vesuvius. J Petrol 34:383–425

Santacroce R, Cioni R, Civetta L, Marianelli P, Métrich N, Sbrana A (1994) How Vesuvius works. In "large explosive eruptions". Atti Conv Acc Naz Lincei 112:185–196

Scandone R, Giacomelli L, Fattori Speranza F (2008) Persistent activity and violent strombolian eruptions at Vesuvius between 1631 and 1944. J Volcanol Geothermal Res 170:167–180

Schmincke HU (2004) Volcanism. Springer, Berlin

Sheridan MF, Barberi F, Rosi M, Santacroce R (1981) A model from Plinian eruptions of Vesuvius. Nature 289:282–285

Sneed ED, Folk RL (1958) Pebbles in the lower Colorado River, Texas, a study in particle morphogenesis. J Geol 66:114–150

Sparks RSJ (1978) The dynamics of bubble formation and growth in magmas: a review and analysis. J Volcanol Geotherm Res 3:1–37

Sparks RSJ (1986) The dimensions and dynamics of volcanic eruption columns. Bull Volcanol 48:3–15

Sparks RSJ (1997) Causes and consequences of pressurization in lava dome eruptions. Earth Planet Sci Lett 150:177–189

Sparks RSJ, Bursik M, Ablay GJ, Thomas RME, Carey SN (1992) Sedimentation of tephra by volcanic plumes. Part 2: controls on thickness and grain-size variation of tephra fall deposits. Bull Volcanol 54:685–695

Stormer JC Jr, Nicholls J (1978) XLFRAC: a program for the interactive testing of magmatic differentiation models. Comput Geosci 4:143–159

Stothers BR, Rampino RM (1983) Volcanic Eruptions in the Mediterranean before A.D. 630 from written and archaeological sources. J Geophys Res 88:6357–6371

Stothers RB (1984) The great Tambora eruption in 1815 and its aftermath. Science 224:1191–1198

Sulpizio R, Mele D, Dellino P, La Volpe L (2005) A complex, Subplinian-type eruption from low-viscosity, phonolitic to tephri-phonolitic magma: the AD 472 (Pollena) eruption of Somma-Vesuvius, Italy. Bull Volcanol 67:743–767. doi:10.1007/s00445-005-0414-x

Varekamp JC (1993) Some remarks on volcanic vent evolution during plinian eruptions. J Volcanol Geotherm Res 54:309–318

Walker GPL, Croasdale R (1972) Characteristics of some basaltic pyroclastics. Bull Volcanol 35:303–317

Wilson L, Sparks RSJ, Walker GPL (1980) Explosive volcanic eruptions-IV. The control of magma properties and conduit geometry on eruption column behaviour. Geophys J R Astron Soc 63:117–148

Wohletz KH (1986) Explosive magma-water interactions: thermodynamics, explosion mechanisms and field studies. Bull Volcanol 48:245–264

Wohletz KH (2000) Were the Dark Ages triggered by volcano-related climate changes in the 6th Century? Eos Trans. AGU 81(48), Fall Meet Suppl

Wohletz KH, Sheridan MF, Brown WK (1989) Particle size-distributions and the Sequential Fragmentation/Transport theory applied to volcanic ash. J Geophys Res 94:15703–15721

Wong LJ, Larsen JF (2010) The Middle Scoria sequence: a Holocene violent strombolian, subplinian and phreatomagmatic eruption of Okmok volcano, Alaska. Bull Volcanol 72:17–31

Wylie JJ, Voight B, Whitehead JA (1999) Instability of magma flow from volatile-dependent viscosity. Science 285:1883–1885